17th Annual

VANDERBILT POSTDOCTORAL ASSOCIATION SYMPOSIUM

Program

November 17, 2023 | VU Student Life Center

Sponsored by the Office of Postdoctoral Affairs

Table of Contents

Foreword

2023 VPA Scholarly Learning Co-Chairs

Dr. Madeline Searcy Dr. Madushika Wimalarathne

The Vanderbilt Postdoctoral Association (VPA) was founded in 1998 as a mechanism to support the professional, personal, and scholarly success of postdocs from Vanderbilt University and Vanderbilt University Medical Center. Since then, the VPA has organized 16 annual symposia, highlighting the works of hundreds of previous postdoctoral scholars. Over this past year, we have had a dedicated group of postdocs from both VU and VUMC working together to make our 17th Annual VPA Symposium an interactive experience for postdocs who call Vanderbilt home.

The symposium planning committee has worked to cultivate an exciting program of content that includes research from a diverse array of departments, including Medicine, Earth and Environmental Sciences, Electrical and Computer Engineering, and Physics and Astronomy. The day of events is broken into two poster sessions, a single lightning talk session, a career advising session, a concurrent moderated panel discussion by both academic faculty and non-faculty early career scientists and Vanderbilt alumni, and of course, our keynote address and lunch. We are also excited to have our Resource Fair, which will include campus organizations that provide services for postdocs across VU and VUMC.

We would like to thank all of our presenters, our invited speakers, Dr. Kevin Stassun and Dr. Ashley Brady, our panel members, and, of course, our university sponsors, the Office of Postdoctoral Affairs and the Office of Biomedical Research Education and Training, all without whom this symposium would not be possible.

In closing, on behalf of the Vanderbilt Postdoctoral Association and the symposium planning committee, we hope this day brings opportunities for scientific discovery, collaboration, and networking!

Schedule of Events

All events are in Central Standard Time (CST)

9:00 am - 9:15 am	**Welcome Remarks by Dr. André Christie-Mizell** Vice Provost for Graduate Education, Dean of the Graduate School, Director of the Office of Postdoctoral Affairs
9:15 am - 9:45 am	**Research talk by Dr. Siru Liu** 2023 Postdoc of the Year
10:00 am - 10:45 am	**Poster Session A** **Campus Resource Fair**
10:45 am - 11:00 am	**Break**
11:00 am - 11:30 am	**BRET Office Talk by Dr. Ashley Brady**
11:30 am - 1:00 pm	**Lunch** **Keynote Address by Dr. Keivan Stassun** Stevenson Professor of Astrophysics, College of Arts & Science Professor of Computer Science, Vanderbilt School of Engineering Director, Frist Center for Autism and Innovation at Vanderbilt
1:15 pm - 2:15 pm	**Academic Alumni Panel** **Dr. Andrew Wiese**, Health Policy **Dr. Deanna Edwards**, Rheumatology and Immunology **Dr. Eric Wilkey**, Psychology and Human Development **Non-Academic Track Alumni Panels** **Dr. Shanna A. Arnold Egloff**, HCA Healthcare Research Institute **Dr. Jesse Spencer-Smith**, Data Science Institute at Vanderbilt University **Dr. Thomas W. Doub,** Center for Patient and Professional Advocacy at Vanderbilt University
2:30 pm - 3:15 pm	**Poster Session B** **Campus Resource Fair**
3:15 pm - 3:30 pm	**Break**
3:30 pm - 5:00 pm	**Lightning Talk Presentations**
5:00 pm - 5:30 pm	**Closing Remarks** **Award Ceremony & Social**

VU Student Life Center

310 25th Ave. S.

Nashville, TN

37240

Public parking is available at the 25th Ave garage, located within walking distance from the SLC.

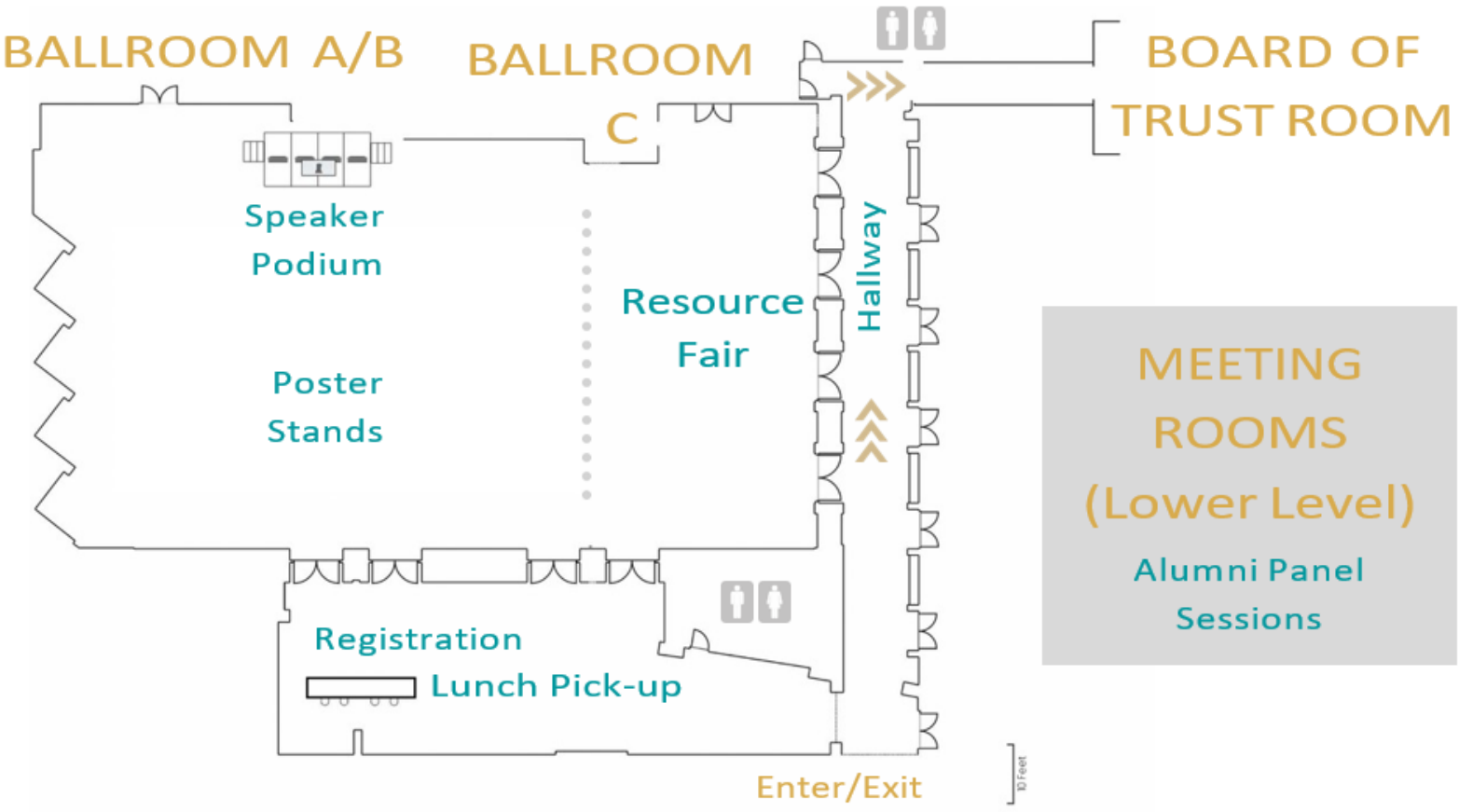

REGISTRATION

Please check-in at the registration desk to get your name badge and lunch/drink tickets (applicable to those who pre-registered).

2023 Postdoc of the Year

9:15 AM - 9:45 AM

Ballroom AB

Dr. Siru Liu

Assistant Professor

Department of Biomedical Informatics

Vanderbilt University Medical Center

Generative AI and Large Language Models in Healthcare: Potentials, Challenges, and Ethical Considerations

Electronic health records (EHR) have significantly transformed the storage and accessibility of medical information. The large amount of medical data provides the foundation for improving healthcare quality through cutting-edge information technology, such as AI. Within EHR systems, clinical decision support (CDS) tools and patient portals play key roles. In this talk, Dr. Siru Liu will highlight the potential of integrating generative AI and large language models in healthcare. Dr. Liu highlights two cases and concludes with ethical considerations for using generative AI in healthcare:

1. Assessing the Value of ChatGPT for CDS Optimization, and
2. Leveraging Large Language Models for Generating Responses to Patient Messages.

Keynote Address

11:30 AM - 1:00 PM

Ballroom AB

Dr. Keivan G. Stassun

Stevenson Professor of Physics & Astronomy
Director, Frist Center for Autism & Innovation
Founding Director, Fisk-Vanderbilt Masters-to-PhD Bridge Program

Vanderbilt University

Head in the Stars, Feet on the Ground: Building on Where You Came From to Get Where You're Going and Make a Difference

The past decade has witnessed an explosion in our understanding of the diversity of other worlds that populate the universe. We will describe Vanderbilt's role in the development of the space telescope missions that are driving this revolution, the diverse human talents that make these discoveries possible, and some personal reflections on building a scientific career of purpose and meaning.

Alumni Panels

1:15 – 2:15 PM

SLC Meeting Rooms 1 & 2

Non-Academic Track Panel

Moderated by Dr. Jessica Abner

Senior Career Coach, Career Center

Dr. Shanna A. Arnold Egloff

Director, Records Based Research, HCA Healthcare Research Institute

Dr. Jesse Spencer-Smith

Interim Director, Chief Data Scientist, Data Science Institute
Vanderbilt University

Dr. Thomas W. Doub

Vanderbilt Center for Patient and Professional Advocacy, Vanderbilt University

Academic Track Panel

Moderated by Dr. Jessica Abner

Senior Career Coach, Career Center

Dr. Andrew Wiese

Assistant Professor, Department of Health Policy

Dr. Deanna Edwards

Assistant Professor, Rheumatology and Immunology

Dr. Eric Wilkey

Assistant Professor, Psychology and Human Development

Career Advising Session

11:00 - 11:30 AM

Ballroom AB

Taking Flight: Assessing the timeline for beginning the job search and exiting your postdoc

When you are in a postdoctoral training position, knowing when to start the job search can seem daunting. Determining when you have sufficient credentials to be competitive for the position you are seeking is only half the challenge. You may also be wondering when you should start the search to be able to obtain a position at a particular time and what steps you should be taking along the way to ready yourself. This session will be focused on helping to answer some of these questions by providing general timelines and considerations for several different common career trajectories, as well as a framework for you to think objectively about your own career path and timeline. Resources for helping you prepare will also be shared so you can make the most of your time as postdoc and set yourself up for a successful transition to your next role.

Dr. Ashley Brady

Assistant Dean of Biomedical Career Engagement and Strategic Partnerships
Associate Professor of Medical Education and Administration
Office of Biomedical Research Education and Training (BRET)

Resource Fair

Session A (10:00 - 10:45 AM) | Session B (2:30 - 3:15 PM)

Ballroom C

Resources

Field Specific	**Session**
Biostatistics Collaboration Center	A, B
BRET ASPIRE Program	A, B
CISR Core (Cell Imaging Shared Resource)	A, B
Office of Research (VUMC)	A
VANGARD (Vanderbilt Technologies for Advanced Genomics Analysis and Research Design)	A, B
VANTAGE (Vanderbilt Technologies for Advanced Genomics)	A, B
VICTR (Vanderbilt Institute for Clinical and Translational Research)	A, B
Identity Affinity Groups	
Bishop Joseph Johnson Black Cultural Center	A
Center for Spiritual and Religious Life	A, B
Margaret Cuninggim Women's Center	A
Office of LGBTQI Life	A, B
Professional Development	
Career Center	A, B
Creative Data Solutions	A, B
Graduate and Postdoc Academic Success (GPAS)	A, B
Graduate Leadership Institute	A, B
University Libraries	B
Writing Studio	B
Edge for scholars	A, B
Center for Technology Transfer and Commercialization	A, B

Resource Fair

Session A (10:00 - 10:45 AM) | Session B (2:30 - 3:15 PM)

Ballroom C

Resources – continued

Health and Wellness	
Health and Wellness (VU)	A
Project Safe (VU)	A, B
Reproductive Health and Parenting (VU)	
The SHARE Center (VUMC)	A, B
Work/Life Connections (VUMC)	A, B
Vanderbilt Credit Union	A, B
International Student Resources	
International Student Scholar & Support (VU)	A
Office of Immigration Service (VU)	A, B
English Language Center	A, B
Vanderbilt Safety Departments	
Vandy Safe	A, B
VUPD and OEM	A, B

Lightning Talks

3:30 - 5:00 PM

Ballroom AB

Select postdocs will present their research through a brief oral presentation, which will be judged by the audience members at the symposium. Two talks with the most popular votes will receive an award at the closing event.

Presenters are listed in alphabetic order.

Dr. Brandon Baer, Vanderbilt University Medical Center
Overexpression of Alveolar Epithelial Tissue Factor Promotes Maintenance of Lung Barrier Integrity in ALI

Dr. Carl Johnson Jr., Vanderbilt University Medical Center
Evaluation of a Novel Cannula for Durable Venovenous Extracorporeal Membrane Oxygenation Using an Ex Vivo Heart Model

Dr. Hunter Robinson, Vanderbilt University Medical Center
Refinement and External Validation of a Novel, Non-Invasive, Multiplex Urine Test for High-Grade Prostate Cancer

Dr. Neelima Wagley, Vanderbilt University
Brain specificity during sentence processing in Spanish-English bilingual children

Dr. Taseer Ahmad, Vanderbilt University Medical Center
Cell Activator protein 1 Mediates Salt-sensitive Hypertension in Humans

Dr. Timothy R. Harris, Vanderbilt University Medical Center
Development of an Ex Vivo Heart Perfusion Platform to Assess Porcine Cardiac Function After Donation After Circulatory Arrest: Lessons Learned in Design

Poster Sessions

Session A
10:00 - 10:45 AM

Session B
2:30 - 3:15 PM

Ballroom 3

Poster presentations will be judged by faculty members and the symposium attendees.
Four posters with the highest scores will receive an award.

Presenters are listed in a random order.

Poster Session A

1A. Food restriction influences action control strategies and dopamine release in the dorsal striatum of mice
Maxime Chevee

3A. Longitudinal local and peripheral immunologic changes identify immune checkpoint inhibition response signatures in murine breast cancer models
Ann Hanna

5A. The evolutionary design of an oligomeric ATPase machine
Subu Subramanian

7A. Shareholder Value Maximization, Ownership Heterogeneity and Vulnerability
Leon Anidjar

9A. Activation Mechanisms for Context-Dependent Allosteric Modulation of the mGlu7 receptor
Xia Lei

11A. Black Cosmopolitans: Borders and Asylum from the Eighteenth Century Caribbean to Present-Day Tijuana, Mexico
Jesus Ruiz

13A. Engineered RIG-I Activating Nanoparticles Attenuate Glioblastoma in Mice
Alexander Kwiatkowski

15A. NeuroGraph: Benchmarks for Graph Machine Learning in Brain Connectomics
Anwar Said

17A. Intramolecular interactions that stabilize factor XII in a closed form
Aleksandr Shamanaev

19A. Activity dependent Clustering of Neuronal L-Type Calcium Channels by CaMKII
Qian Yang

Poster Sessions

Session A
10:00 - 10:45 AM

Session B
2:30 - 3:15 PM

Ballroom 3

21A. Positive Allosteric Modulation of the M1 Muscarinic Acetylcholine Receptor via Tool Compound VU0486846 Prolongs Survival and Improves Cognition in Neurodegenerative Diseases
Daniel Schultz

23A. Feasibility of Systemic Radiotracer for Pre-operative Staging and Sentinel Lymph Node Biopsy in Head and Neck Cancer
Nicole Meeks

25A. Hepatic specific Cholesteryl Ester Transfer Protein regulates Metabolic Associated Fatty Liver Disease by sex dimorphism
Sivaprakasam Chinnarasu

27A. Prediction Models for Incidence Tuberculosis in Contacts of People with Tuberculosis: A Systematic Review
María B. Arriaga

29A. Transition metals alloys trigger blood coagulation via intrinsic pathway: implications for intravascular devices
Maxim Litvak

31A. Uncertainty quantification in microstructure images with moment invariants
Arulmurugan Senthilnathan

33A. Size and Stiffness Based Microfluidic Sorting of Metastatic Breast Cancer Cells to Examine Mechanotype Stability and Heritability
Katie Young

35A. Occupational benzene exposure and cancer risk among Chinese men: A report from the Shanghai Men's Health Study
Douglas DeMoulin

37A. The Maya are a People of Movement: An Isotopic Assessment at Chactemal (Santa Rita Corozal), Northern Belize
Angelina J. Locker

39A. Unraveling the genetics underlying the brain function of the rhythm network
Yasmina Mekki

41A. Type 2 diabetes mellitus, its type and blood pressure traits: A two-sample Mendelian randomization study

Poster Sessions

Session A
10:00 - 10:45 AM

Session B
2:30 - 3:15 PM

Ballroom 3

43A. Assessing the glycation effect and mechanical damage in human cortical bone through Raman Spectroscopy
Rafay Ahmed

45A. Targeted Temperature Cooling or Rewarming for Porcine Hearts Procured After Donation After Circulatory Death
Timothy R. Harris

47A. Drug repurposing for Alzheimer's disease: the use of genetics-enriched, neuropathology-associated SPI1 regulon in microglia
Yuting Tan

49A. Polarization sensitive Raman spectroscopic studies for rattail tendon tissue.
Chitra Shaji

Poster Session B

2B. Advancing the Construction of High Spatial Resolution Multimodal Molecular Atlases with the Aid of Data-Driven Image Fusion
Olof Gerdur Isberg

4B. Whole Foods for Prediabetes: Feasibility and Acceptability of a Dietary Guidelines-Based Intervention for Type 2 Diabetes Prevention in Families
Nadia M. Sneed

with Epileptic Encephalopathy
Kirill Zavalin

8B. Characterization of Mycobacterium Tuberculosis – Bacillus Calmette-Guerin Using Surface Enhanced Raman Spectroscopy
Timothy W. Yokley

10B. Genetically determined body fat percentage affects kidney function via the proteome
Jefferson L. Triozzi

12B. Fast Fuzzy C-Means Segmentation for Keypoint based Differentiation of Homogenous and Speckled Cellular Shapes
Kanchana Devanathan

14B. Social Experiences and Mental Health Outcomes Among Autistic LGBTQ+ Youth
Natalie Libster

Poster Sessions

Session A
10:00 - 10:45 AM

Session B
2:30 - 3:15 PM

Ballroom 3

16B. Privacy-preserving collection and sharing of unbiased human voice data for automatic assessment of voice disorders
Zhiyu Wan

18B. Adolescent-onset voluntary ethanol consumption and subsequent negative affective behavior and whole brain cFos expression during forced abstinence in mice
Caitlyn Edwards

20B. Correlates of Self-Reported Life Satisfaction in Autistic Youth with and without Intellectual Disability
Carly Moser

22B. Static storage at 10°C improves biliary viability in porcine donation after cardiac death livers
Kaitlyn M. Tracy

24B. Rapid handheld measurements of skin and subcutaneous tissue stiffness in Systemic Sclerosis: a case series
Shramana Ghosh

26B. Proteomic Alteration in T1DM: Insights into Cardiometabolic Complications and Hyperinsulinemia-Driven Insulin Resistance
Naweed Akbar

28B. Neurobiological Underpinnings of Discourse Understanding: Integra7ve Insights from fMRI and EEG
Clair Hong

30B. Effect of Pediatric Doses of Atomoxetine on Presyncope Symptoms in Neurogenic Orthostatic Hypotension: A Randomized, Double-blind, Placebo-Controlled, Crossover, Clinical Trial
Naome Mwesigwa

32B. Imaging of Metabolites in Human Ocular Tissue by Mass Spectrometry
Ali Zahraei

34B. Glutaminase Promotes Amino Acid-Induced Alpha Cell Proliferation
Madushika Wimalarathne

36B. Dynamic organ storage at 10°C improves cholangiocyte function compared to static cold storage
Yutaka Shishido

Poster Sessions

Session A
10:00 - 10:45 AM

Session B
2:30 - 3:15 PM

Ballroom 3

38B. The EaRTH Disk Model: Analyzing Millimeter and Infrared Observations of Disk Substructures of Transitional Disks
William Grimble

40B. Cognitive empathy anosognosia relates to social vulnerability in behavioral-variant frontotemporal dementia
Jayden J. Lee

42B. Elucidating the Role of Activated Leukocyte Cell Adhesion Molecule (ALCAM) in the Biogenesis and Function of Tumor Extracellular Vesicles
Javier Ramirez-Ricardo

44B. Intralaboratory Evaluation of a Quality Control Workflow across Identical LC-MS/MS Systems
Khiry L. Patterson

46B. Understanding the role of TET2-deficient monocytes in clonal hematopoiesis of indeterminate potential (CHIP)
Kristen Dickerson

Abstracts
Lightning Talks

Overexpression of Alveolar Epithelial Tissue Factor Promotes Maintenance of Lung Barrier Integrity in ALI

Brandon Baer

Acute Respiratory Distress Syndrome (ARDS) is a common cause of acute respiratory failure. Despite extensive research in animal models, in which the syndrome is called Acute Lung Injury (ALI), no targeted therapy has been found to reduce its high mortality rate. Two major pathologic features of ARDS are loss of lung barrier integrity and activation of the Tissue Factor (TF) pathway of coagulation in the airspace. However, as an integral membrane protein TF also serves several non-coagulant functions including promotion of cell adhesion. All systemic anticoagulants tested have failed to show clinical benefits in ARDS, with some trials of TF pathway inhibition showing increased mortality in ARDS patients. One explanation for these clinical results is that **TF in the airspace is protective in ARDS**. Supporting this concept, our previously published mouse work found that loss of alveolar epithelial cell TF caused increased loss of lung barrier integrity in models of ALI. As such, we hypothesize that epithelial TF is necessary for maintaining lung barrier integrity and that its overexpression will be protective in ALI. To determine whether supraphysiologic overexpression of TF in the lung can enhance barrier integrity we created a novel transgenic mouse in which TF was inducibly overexpressed in the lung epithelium (TFEpi+). Specifically, a human influenza hemagglutinin-tagged TF construct, driven by the CMV-TetO promoter and crossed with SPC-rtTA59 mice was used to produce inducible, lung epithelial-targeted TF overexpressing mice. High alveolar epithelial TF expression compared to wild-type littermates (WT) was confirmed through immunohistochemistry and western blot analysis after one week of doxycycline in drinking water. To induce ALI, mice were intranasally infected with 2000 colony forming units of Klebsiella pneumoniae or PBS. At 24-hours post infection, mice were euthanized, lung tissue was collected, and a bronchoalveolar lavage (BAL) was performed. Animal body weights were recorded pre-, and 24-hours post infection. BAL was analyzed to measure protein, clot time, and leukocyte influx. Lung tissue was utilized to calculate wet-to-dry weight ratios and bacterial burden. TFEpi+ mice infected with Klebsiella pneumonia showed lower BAL protein (366.3 vs 254.8 µg/ml; n=15-19; p=0.0035) and lung wet-to-dry weight ratios (5.482 vs 4.826; n=15-19; p=0.0328) compared to WT However, weight loss, bacterial burden, and BAL clot time did not differ between infected TFEpi+ and WT mice. These findings suggest that alveolar epithelial TF overexpression is protective for maintaining lung barrier integrity and a non-coagulate based mechanism, potentially linked to epithelial cell adhesion.

Evaluation of a Novel Cannula for Durable Venovenous Extracorporeal Membrane Oxygenation Using an Ex Vivo Heart Model

Carl Johnson Jr.

Objective: Fifteen million Americans suffer from chronic obstructive pulmonary disease (COPD). After failed optimal medical therapy, the only definitive treatment is lung transplantation, which is limited due to donor scarcity. Extracorporeal membrane oxygenation (ECMO) can be used in COPD exacerbations, but it is not designed for long-term respiratory support. Existing venovenous (VV.) ECMO configurations often utilize a dual lumen cannula that can demonstrate high resistance and hinder patient ambulation. We are developing a dual lumen cannula that attaches to the heart and is tunneled to an ergonomic position that could provide durable, long term ECMO support. We describe here an ex vivo heart model to evaluate the pressure flow relationship of this novel cannula and to assess and optimize its surgical attachment and anatomical fit. Methods: A novel cannula for long-term VV ECMO support was designed for surgical attachment to the right atrium. En bloc porcine heart-lung specimens were obtained from a local slaughterhouse. The heart was dissected from the specimen while preserving maximal pulmonary artery length. We performed a pulmonary artery-to-superior vena cava end-to-end anastomosis. The inferior vena cava and the coronary sinus were suture ligated. The novel cannula was attached to the right atrium and connected to a circuit containing a centrifugal blood pump to establish a closed right heart circuit (Figure 1, N=5). The circuit was primed with deionized water at ambient temperature. A circuit using a venous reservoir was constructed as a control group to the ex vivo model (N=10). Pressure drop between the reservoir and each cannula port was assessed for both drainage and reinfusion at flow rates between 0.25 – 5LPM. Results: The novel cannula drainage pressure drop (-36.4±0.2mmHg) on the ex vivo circuit was less than the pressure drop in the venous reservoir (-27.7±1.3mmHg) at 3LPM (Figure 2). Reinfusion pressure drop was higher in the ex vivo circuit (52.2±0.7mmHg) compared to the venous reservoir circuit (45.5±1.4mmHg) at 3LPM. Total pressure drop was higher in the ex vivo circuit (88.6±0.7mmHg) compared to the venous reservoir (73.2±2.2mmHg) at 3LPM. Conclusions: The overall pressure drop was greater in the ex vivo heart circuit suggesting that it may provide a more realistic assessment of the pressure flow relationship of a novel cannula as opposed to a venous reservoir. This ex vivo heart model provides a more rigorous platform for cannula fit testing and pressure flow assessment prior to initiating in vivo studies.

Abstracts
Lightning Talks

Refinement and External Validation of a Novel, Non-Invasive, Multiplex Urine Test for High-Grade Prostate Cancer.

Hunter Robinson

Importance: Prostate cancer is the second leading cause of cancer death in American men. Benefits of screening with serum prostate-specific antigen (PSA) are largely offset by a high rate of negative biopsies and overdetection of indolent cancers resulting from the poor specificity of PSA for higher-grade, clinically significant cancers. Objective: To develop an expanded multiplex urinary panel for clinically significant (grade group [GG]≥2) prostate cancer and evaluate diagnostic performance in an external validation cohort relative to current guidelineendorsed biomarker tests. Design, Setting, and Participants: RNA sequencing analysis of 58,724 genes identified 54 markers of prostate cancer, including 17 novel markers uniquely overexpressed by GG≥2 cancer. The optimal model of gene expression plus standard clinical factors (MyProstateScore2.0 [MPS2]) and a parallel model incorporating prostate volume (MPS2+) for GG≥2 cancer were derived in an institutional development cohort (n=761). The locked MPS2 models underwent blinded, external validation in a prospective National Cancer Institute trial cohort (n=743) referred for biomarker testing and biopsy. All patients underwent protocolized urine collection and transrectal ultrasound-guided prostate biopsy at enrollment. Main Outcome(s) and Measure(s): Multiple biomarker tests were assessed in the validation cohort, including PSA, Prostate Cancer Prevention Trial risk calculator (PCPTrc), prostate health index (PHI), derived multiplex SelectMDx (mxSMDx) and ExoDx Prostate Intelliscore (mxEPI), the original two-gene MyProstateScore (MPS) model, and the locked 18-gene MPS2 models. The area under the receiver operating characteristic curve (AUC) for GG≥2 cancer was derived for each test. Under a clinically pertinent testing approach with 95% sensitivity for GG≥2 cancer, the specificity, negative predictive value (NPV), and positive predictive value (PPV) of each test was calculated in the initial and repeat biopsy settings. GG≥3 was secondarily assessed. Results: The validation cohort included 743 men (median age 62 years; median PSA 5.6 ng/mL), of which 151 (20%) were found to have GG≥2 cancer on biopsy. The AUC was 0.597 for PSA, 0.659 for the PCPTrc, 0.772 for PHI, 0.761 for mxSMDx, 0.716 for mxEPI, and 0.737 for MPS, as compared to 0.818 for the optimal MPS2 model. At 95% sensitivity for GG≥2 cancer, the optimal MPS2 model provided clinically significant improvements in specificity in the initial biopsy (42% vs. 27%, 30%, 30%, 17%, and 27% for PCPTrc, PHI, mxSMDx, mxEPI and MPS, respectively) and repeat biopsy (51% vs. 21%, 8.7%, 14%, 16% and 15% for PCPTrc, PHI, mxSMDx, mxEPI and MPS, respectively) settings. Across all pertinent clinical subgroups, MPS2 provided ≥95% NPV for GG≥2 cancer and 99% NPV for GG≥3 cancer. Conclusions and Relevance: In a large, external population referred for prostate biopsy, the novel MPS2 test improved detection of GG≥2 cancer on direct comparison with current biomarker tests. Clinically, MPS2 testing would reduce the frequency of unnecessary biopsies performed while maintaining highly sensitive detection of clinically significant cancers. These data support the use of MPS2 in men with elevated PSA to reduce the potential harms of prostate cancer screening while preserving its long-term benefits.

Brain specificity during sentence processing in Spanish-English bilingual children

Neelima Wagley

How does bilingualism influence functional specialization of the language network in the brain? Comprehending a sentence requires the integration of both syntactic and semantic information and relies on a distributed network of brain regions involved in these processes. Individual variations in language experience, such as early exposure to two languages, influence this dynamic process. This study is the first to investigate Spanish-English bilingual children's functional brain organization for syntactic and semantic language processes in English, their primary language of academic instruction. Sixty-five children ages 7 to 11(M=8.6 years old) who were exposed to Spanish from birth and English before age five participated in the study. They completed language assessments in both English and Spanish while parents completed background questionnaires. Families were recruited from a geographical region of the US that is composed of majority White and English-dominant communities. We examined specificity for syntax and semantics using two auditory sentence judgement tasks during functional near infrared spectroscopy (fNIRS), a developmentally friendly brain imaging methodology. In the experimental tasks, participants heard a sentence and indicated whether it was semantically plausible or grammatically correct (60 trials per task). The morphosyntax task elicited activation in left inferior frontal gyrus (IFG) and the semantic task elicited activation in left posterior middle temporal gyrus (MTG), in line with prior research on English monolingual children. Task comparisons revealed specialization in left superior temporal (STG) for morphosyntax and left MTG and angular gyrus for semantics. Although skills in neither language were uniquely related to specialization, skills in both languages were related to engagement of the left MTG for semantics and left IFG for syntax. Theories of bilingualism posit that children's experiences with the two languages make a combined contribution to their language development. Our results are consistent with prior neurocognitive language models suggesting a positive cross-linguistic interaction in those with higher language proficiency.

Abstracts
Lightning Talks

Antigen Presenting Cell Activator protein 1 Mediates Salt-sensitive Hypertension in Humans

Taseer Ahmad

Salt-sensitivity of blood pressure (SSBP) is defined by the changes in blood pressure according to dietary sodium loading/depletion and is a major independent risk factor for morbidity and mortality due to cardiovascular disease, even in normotensive individuals. We previously found that SSBP is associated with activation of antigen presenting cells (APCs), but the underlying mechanisms are unknown. The activator protein 1 (AP-1) (Fos/Jun) has been implicated in mediating inflammation but its role in SSBP is not known. We hypothesized that AP-1 in APCs senses elevated sodium and contributes to SSBP. Using bulk RNA-sequencing in human monocytes, we found elevated sodium increases expression of the AP-1 gene family when compared to normal sodium concentration, including FOS (2378.18 ± 480.7 vs 6494.09 ± 945.55, p= 0.0009), FOSB (47.63 ± 17. 55 vs 56.06 ± 10.30, p= 0.5320), JUN (7313.90 ± 984.93 vs 11370.09 ± 1286.35, p= 0.2563) JUNB (4745.36 ± 599. 17 vs 5955.45 ± 600.91, p= 0.7620) and JUND (3309. 63 ± 270.64 vs 8057.90 ± 1043.05, p= 0.00006). In additional experiments, we enrolled people with hypertension and phenotype them for SSBP using an established in-patient protocol of salt-loading/depletion and performed single-cell transcriptomic analyses in vivo on PBMCs. We found that expression of the FOS and JUN genes change in concert with blood pressure after salt-loading and depletion in salt-sensitive but not salt-resistant humans. Our findings reveal a role for immune cell AP-1 signaling in salt sensitive hypertension and may provide a potential target for treatment and diagnosis.

Development of an Ex Vivo Heart Perfusion Platform to Assess Porcine Cardiac Function After Donation After Circulatory Arrest: Lessons Learned in Design

Timothy R. Harris

Background: Ex vivo heart perfusion (EVHP) is a platform used to perfuse, preserve, and assess donor hearts in a beating state. EVHP platforms have both clinical and research application in heart transplantation, such as the Transmedics OCSTM or PhysioHeartTM platforms. Their cost is often prohibitive for research, and a means to design an economic, noninferior platform warrants consideration. The aim of this study is to design a cost-effective, non-inferior EVHP platform for porcine cardiac allografts. Methods: Inclusion criteria for our EVHP platform included the following: reservoir, pump, oxygenator, heater, dual circuit pathways to allow for either retrograde or antegrade flow, priming and de-airing arms. Circuit success was defined as: perfusate exchanges occur without air or hemodilution, physiologic coronary flow and aortic pressures achieved, normothermia achieved, volume required <1L, and capacity to re-animate the heart. Secondary variables included lack of hemolysis or clot. Iterative circuit re-design was performed based on achieving or failure to achieve these criteria. Results: N=6 circuit iterations were performed. Swine hearts (335 + 93.7g) procured after circulatory arrest were utilized. Circuits were primed with heparinized autologous blood. 4/6 circuits demonstrated flow, however, early circuits resulted in aortic insufficiency. 2/6 achieved coronary flow while maintaining aortic valve competence. 1/6 achieved normal aortic pressure and coronary flow (45mmHg and 0.8mL/g/min, respectively). These circuits additionally could de-air and prime during flow without incurring hemodilution. The sixth iterative circuit achieved all criteria except for cardiac reanimation. Plasma free hemoglobin, a marker of hemolysis, notably decreased from 78.5 to 56.92 on assay. Aortic thermography was 36oC during reperfusion. Notable factors in the current circuit iteration included: elevated de-airing limb proximal to the aorta, heart suspended to maintain taut valve, >20 Fr aortic cannula, a low-volume reservoir, an oxygenator at the height of the heart, and a modified angle of tubing to achieve a desired aortic pressure. Functional reanimation, however, was not observed in current porcine hearts. Conclusion: We have created an EVHP platform that permits coronary flow with normal aortic pressures. This platform allows for de-airing, perfusate exchange without hemodilution or inducing air into the circuit and achieves normal aortic root pressures and coronary flow. Failure of cardiac re-animation is hypothesized to be secondary to hyperkalemia and hypocalcemia. Further iterative changes include perfusate electrolyte normalization, cardiac defibrillation with electrical pacing, and utilization of antegrade flow

Abstracts
Poster Presentations

Poster Session A

1A. Food restriction influences action control strategies and dopamine release in the dorsal striatum of mice
Maxime Chevee

Diverse factors influence how we control our actions. For example, reinforcement schedules bias control strategies via distinct action-outcome contingencies. However, non-learning related factors have equally important influences on behavior and must be studied in combination with reinforcement principles to understand how animals learn and control their actions. One such factor is food deprivation – a condition often experimentally induced to enhance task engagement and learning rate in operant training. While restricting caloric intake is known to affect general states such as motivation and stress, whether and how it specifically changes action control strategies is not well understood. The goal of this study is to determine the neural mechanisms that underlie the influence of food restriction on action control strategies. 1) We first induced different levels of food restriction in male and female mice and showed that stricter food restriction during training on a random interval schedule results in behaviors that are more sensitive to extinction. This finding indicates food restriction promotes a goal-directed strategy and suggested that dorsomedial (DMS) and dorsolateral (DLS) striatum dopamine may be differentially affected. 2) To test this hypothesis, we measured dopamine release in striatal slices using voltammetry. We found that food restriction increased dopamine release in DMS but not in DLS. This result suggested that food restriction promoted changes in the regulation of dopamine release at axon terminals. 3) Similarly, in vivo fiber photometry recordings using the dopamine sensor dLight revealed that food restriction modulated dopamine release in DMS, but not DLS. Surprisingly, only the response to sucrose consumption was increased, whereas the responses to randomly delivered external stimuli were not affected by food restriction. This finding raised the question: how could terminal regulation differentially impact dopamine released in response to distinct external events? Our voltammetry and fiber photometry data suggest that modulation by food restriction state change terminal release in a way that is only apparent when large amounts of dopamine are released. Thus, we hypothesized that food restriction changes the expression of the dopamine transporter (DAT), which normally works to blunt the size of large dopamine transients and controls re-uptake dynamics. 4) Consistent with our hypothesis, we found that expression of a phosphorylated version of DAT (T53) was reduced specifically in DMS under food restriction conditions. Thus, our study shows that food restriction fundamentally affects behavioral control strategy and the balance of dopamine release in dorsal striatum. Specifically, our data suggest that food restriction reduces the efficiency of dopamine re-uptake by DAT via phosphorylation of the T53 residue specifically in DMS. This leads to enhanced dopamine release in DMS compared to DLS, thus promoting DMS-dependent goal-directed control of actions. We are currently performing several experiments to test predictions that stem from these observations and to determine whether DAT phosphorylation, enhanced dopamine release and behavioral changes are causally linked.

3A. Longitudinal local and peripheral immunologic changes identify immune checkpoint inhibition response signatures in murine breast cancer models
Ann Hanna

Background: Immune activating checkpoint inhibitors (ICI) improve patient survival in many cancer types with limited success in breast cancer. Phase-III clinical trials in triple-negative breast cancer (TNBC) patients report increased pathologic complete response. Despite FDA approval of ICI combinations with standard-of-care chemotherapy, many patients treated are resistant to ICI, and the underlying mechanisms of resistance and their diversity are poorly understood. Objective: Identifying reliable in vivo models to evaluate therapeutic resistance, heterogeneity in response, synergistic therapeutic efficacy, and predictive biomarkers for response to ICI. Methods: Using an immunocompetent mammary tumor EMT6 model, we investigated the efficacy of aPD-L1. The primary tumor cellular microenvironment and peripheral blood from mice with differential responses were longitudinally assessed by single-cell (or bulk) RNA sequencing and T-cell receptor sequencing, respectively, to identify systemic genetic alterations and T-cell expansion. Results: Systemic PD-L1 blockade significantly reduced mammary tumor growth in the EMT6 mammary tumor model and promoted dendritic and CD8 T cell infiltration. Similar to clinical findings, favorable response was independent of PD-L1 expression. Combinations of standard-of-care chemotherapy (paclitaxel or doxorubicin) demonstrated modest therapeutic efficacy without potentiating single-agent aPD-L1 benefit. Interestingly, aPD-L1 induced heterogeneous responses, recapitulating clinical patient outcome, denoted by complete response and both acquired and intrinsic resistance. Mice transplanted with previously aPD-L1-treated (resistant) tumors retained heterogeneous responses, indicating that ICI response is dictated by host-intrinsic, rather than tumor-intrinsic factors. Despite using a genetically identical murine tumor model/host, transcriptomic analysis of the primary tumor landscape by fine-needle aspiration showed upregulated cytotoxic T cell response and activation signatures, specifically inflammatory interferon signaling (both at baseline and post aPD-L1 administration) that corresponded to favorable response to ICI. Longitudinal analysis of the peripheral blood uncovered clonal T cell expansion present only in responder mice and modest changes among mice at baseline, particularly myeloid cell recruitment signatures, that progressively deviated by response type (non-responders-vs-responder mice). Blocking myeloid cell recruitment using navaraxin (CXCR1/2 inhibitor) or anti-CSF1R enhanced response to ICI, further suppressing tumor growth and enhancing survival. Conclusions: We describe a heterogeneously ICI-responsive mammary murine model, which reflects heterogeneous patient response to ICI. Longitudinal host-specific signatures, specifically myeloid cells, correlating with differential response to ICI may serve as rationale for tracking ICI response in peripheral blood from breast cancer patients. Ongoing efforts to phenotypically characterize clinical specimens from patients treated with CXCR1/2 inhibitors will elucidate mechanisms responsible for response to ICI and uncover strategies for sensitizing refractory tumors to ICI.

Abstracts
Poster Presentations

5A. The evolutionary design of an oligomeric ATPase machine

Subu Subramanian

Evolution has shaped biological systems to have impressive performance characteristics. Additionally, biological systems display a remarkable tolerance to mutations and yet, can adapt and evolve to meet new challenges. I am interested in elucidating the principles of evolutionary design and will discuss our results from investigating the T4 bacteriophage clamp-loader complex, a protein machine involved in bacteriophage genome replication. We developed a high-throughput mutational perturbation platform for the T4 clamp loader and found the system to be remarkably resilient. To investigate how such robustness enables adaptation to changing environmental conditions, we engineered a chimeric clamp-loader system, resulting in a substantial (~5000-fold) reduction in phage replication rate. Directed evolution experiments uncovered a single mutation to a residue in the core ATP-hydrolyzing module can restore fitness to within ~20-fold of the wildtype system. Systematic mutational studies revealed that substituting multiple DNA-proximal residues with lysine or arginine enhanced the function of the chimeric clamp loader. Collectively, these findings illustrate that the mutationally tolerant protein machine possesses a latent capacity to enhance its affinity for interaction partners, such that even single-point mutations can readily contribute to tuning function in a new context, shedding light on the adaptive potential inherent in natural systems.

7A. Shareholder Value Maximization, Ownership Heterogeneity and Vulnerability

Leon Anidjar

Traditional research on corporate governance (CG) has primarily focused on the agency theory and the shareholder primacy norm, which emphasizes the maximization of shareholder value (Hansmann & Kraakman, 2001; Jansen, 2002), often exemplified by the landmark case of Dodge v. Ford Motor Co. (1919). As a result, the interests of stakeholders are often viewed solely to serve the objectives of stockholders, rather than being given special consideration for firm value creation (Harrison, Phillips & Freeman, 2020). Generally, manager authority over corporate affairs and privileged access to information create risks for misconduct, potentially leaving shareholders vulnerable to adverse outcomes. As a result, shareholder primacy advocates implementing effective mechanisms that mitigate opportunistic behavior by insiders, such as a competitive market for corporate control, diversified institutional investment, robust protections for minority shareholders, and fiduciary duties of the board of directors (Mejia, 2019). The concept of shareholder primacy is justified based on a hypothetical governance bargain among all corporate constituencies, where the prioritization of shareholder interests is seen to maximize the overall wealth (Jensen & Meckling, 1976). Hence, without a clear commitment from directors to maximize shareholder value, stockholders will refrain from delivering capital because they are exposed to the risk of exploitation by other stakeholders who may have more enforceable and specific terms. Moreover, shareholders are the residual risk-bearers, and cost-bearers of insider decision-making and therefore incentivized to exercise oversight over managerial actions (Hansmann, 1988; Sundaram & Inkpen, 2004). In contrast, fixed claimants can generally mitigate risks by specifying predetermined payoffs or incentive structures tied to performance measures by relying on the "contracting interface at which firm and constituencies strike their main bargain" (Williamson, 1985, p. 298; Fama & Jensen, 1983, p. 328). Thus, maximizing the residual value for shareholders, which is the value left after fulfilling the contractual claims of stakeholders, is the efficient solution to promote wealth for all stakeholders involved (Easterbrook & Fischel, 1996). Notwithstanding extensive criticism (Stout, 2012; Partnoy, 2021), the widespread notion among economic theories of the firm (agency and early transaction cost economics theories) is that the primary goal of corporation is to maximize value for shareholder (Lan & Heracleous, 2010; Williamson, 1985), Nevertheless, several important questions are still unresolved suggesting that shareholder primacy is an undertheorized norm. Specifically, four issues require further investigation:

(1) What is the value the corporation must secure for the benefit of shareholders. To discuss maximization in a meaningful way, a clear and one-dimensional objective function is required. However, there is often confusion among scholars who interchangeably use two different notions of value: firm value and shareholder value. If we consider shareholders' equity from the balance sheet as a measure of shareholder value and compare it to firm value, which includes not only equity but also debt or any other financial claims on the corporation, our conclusions about the concept of value and the actions firms should take may vary significantly (Jensen, 2002, p. 236). Furthermore, the concept of maximization is flawed as it is based on theoretical assumptions that are only achievable under unrealistic conditions, including complete voluntary participation, single-price markets, and the absence of market failures such as externalities and monopolies (p. 240). Considering the limitations of bounded rationality and uncertainty, when financial economists refer to the maximization of shareholder value, what they truly mean is that it should be "increased" (Ketokivi & Mahoney, 2017; 2022).

(2) Who are the shareholders whose interests should be prioritized compared to the interests of other corporate constituencies. In particular, the ideology of shareholder primacy rests on the notion that shareholders generally possess homogeneous interests, with goals that are similar, if not identical (Easterbrook & Fischel, 1996). However, the traditional belief in shareholder homogeneity has come under increasing scrutiny due to the emergence of various types of shareholders with diverse interests beyond mere wealth maximization. This undermines the assumptions of agency theory, which assumes uniformity of interests among shareholders. Research has highlighted conflicts among shareholders iindicating that these differing views may override the shared interest in the residual (Goranova & Ryan, 2021).

(3) How the board of directors must increase shareholder value is a central question for corporate governance. Because of the variation in shareholder interests in terms of investment horizons, types, and goals (DesJardine, Zhang & Shi, 2023), insiders are frequently entrusted with the responsibility of addressing, balancing, and prioritizing conflicting demands from diverse investors as part of their efforts to increase shareholder value. This obligation should be accompanied by well-defined governance guidelines and organizational training programs that reinforce the board's

ability to effectively navigate conflicting interests (Klarner, Yoshikawa & Hitt, 2021).
(4) Why recognizing the specific value, a corporation must increase is an essential pursuit for corporate governance research? In our view, acknowledging the tangible value that the board of directors must enhance by navigating and prioritizing the conflicting interests of shareholders (Anidjar, 2022) can provide us with valuable insights into the fiduciary responsibilities of the board of directors towards the shareholders and between the different types of shareholders in different contexts and contingencies (Filatotchev, Ireland & Stahl, 2022; Doh, 2021). Consequently, by integrating the perspectives of both the corporation and the shareholders, we propose a redefinition of the shareholder primacy norm as encompassing (i) the strategic consideration of various types of shareholders, (ii) a trade-off (or prioritization) of conflicting investors' interests, (iii) with the goal of increasing the value of the firm as an independent and separate legal entity.

9A. Activation Mechanisms for Context-Dependent Allosteric Modulation of the mGlu7 receptor
Xia Lei

Metabotropic glutamate receptor 7 (mGlu7) is a dimeric, group III metabotropic glutamate (mGlu) receptor that acts to modulate neurotransmission across many brain structures. mGlu7 is most highly expressed presynaptically in neurons and is widely distributed in the central nervous system (CNS). Mutations, deletions, or decreases in mGlu7 expression result in symptoms and phenotypes of neurodevelopmental disorders in humans and mice, including Rett syndrome. Due to its linkage with human disorders, the receptor may be an ideal candidate for the development of therapeutics. As mGlu7 is one of the eight highly related mGlu receptors, it is difficult to develop compounds with high selectivity when targeting the orthosteric site. For this reason, our group and other are focused on developing ligands that interact with the receptor via an allosteric mechanism to positive or negative modulate orthosteric agonist activity. As the activity of glutamate is very low at mGlu7, the surrogate agonist L-AP4 is often used for compound profiling. We have shown, however, that there are distinctions in the interaction of mGlu7 positive allosteric modulators in the presence of glutamate versus L-AP4. Our current studies extend these findings by profiling the activity of allosteric modulators in the presence of mGlu7-interacting proteins. It is anticipated that understanding the activity of modulators in the presence of these endogenously expressed proteins will be critical to interpretation of native tissue and in vivo effects of mGlu7-targeted modulators.

11A. Black Cosmopolitans: Borders and Asylum from the Eighteenth Century Caribbean to Present-Day Tijuana, Mexico
Jesus Ruiz

In this paper I posit that Christian traditions of religious asylum, should be traced back to the history of the Catholic sanctuary laws in the Spanish Empire. I present cases from the island of Hispaniola in the 1750s in which people of African descent fleeing French and British colonies sought religious sanctuary. Traversing colonial borders and seeking Catholic sanctuary was a method by which African descendants could ostensibly gain their freedom, but it was also made possible by the very fact that these people had lived in borderland spaces. They often acted as pivot points between empires who learned to astutely navigate and utilize a multiplicity of European legal and social systems. Enslaved people seeking refuge and survival became a sort of multilingual hemispheric "cosmopolitan." Thus, one of my principal aims with this paper is to draw a through line from eighteenth century religious sanctuary in the Spanish Caribbean to the ways in which borderlands communities, as well as church organizations in Tijuana, Mexico have provided literal albergues (shelters) to Haitian migrants. I suggest that today's Haitian migrants are part of a long line of African descendant cosmopolitans who spoke a variety of languages and navigated border spaces in their quests for freedom. My hope is to shed light on how both the colonial and current borders of the Americas can function, not just as violent spaces on the peripheries of national cores, but rather as themselves sites of cultural production—a place where an ethos of sanctuary is possible.

13A. Engineered RIG-I Activating Nanoparticles Attenuate Glioblastoma in Mice
Alexander Kwiatkowski

Introduction: Glioblastoma (GBM) is a rare form of brain cancer with over 13,000 new cases each year and a dismal outlook for patients who face a mean survival time of 12-18 months post-diagnosis. Further, there is a high recurrence rate with a five-year survival rate below 10%. The current standard of care – comprising surgical resection followed by radiation and chemotherapy – has not advanced significantly over the past 20 years, creating a need for new therapies. To this end, leveraging pattern recognition receptor (PRR) activation to elicit strong innate immune responses shows promise for cancer immunotherapy. (RIG-I) is one such PRR, and higher levels of RIG-I are associated with improved survival outcomes for the first year following GBM diagnosis. RIG-I recognizes short double-stranded RNA with a triphosphate (3p) group on the 5' end (3pRNA), and RIG-I activation stimulates pro-inflammatory responses, including type-I interferons which trigger antitumor immunity. At the preclinical level, RIG-I activating therapies have shown promise for treating various solid tumors, yet pharmacological activation of RIG-I has not yet been explored for GBM immunotherapy. Despite their promise for cancer immunotherapy, the clinical utility of 3pRNA RIG-I agonists is currently limited by significant drug delivery barriers, including poor intracellular uptake, nuclease degradation in the endosome/lysosome, and an inability to reach the cytosol to bind RIG-I, which we will seek to overcome using RIG-I activating nanoparticles (RANs). Previous data from the lab shows that RANs are taken up by antigen presenting cells where they escape the endosome to deliver cargo to the cytosol overcoming some of the barriers of free RNA delivery. Methods and Materials: Di-block polymer were formed with reversible addition–fragmentation chain transfer (RAFT) polymerization using a first block of 10K polyethylene glycol (PEG) and a second block of poly[(DMAEMA-c-butyl methacrylate (BMA)) (DB). The DB block serves to complex with RNA and enhance endosomal escape. To form micelles, the di-block copolymer was dissolved in ethanol at 100 mg/mL then diluted with sterile-filtered citrate buffer (pH=4.2) to a concentration of 25 mg/mL. RNA was added for 45 minutes at room temperature then dialyzed overnight to concentrate the

solution. Ribogreen (Thermofisher) was conducted according to the manufacturer's protocol to quantify RNA loading. Nanoparticle sizing used dynamic light scatter (DLS) on a Zetasizer Nano ZS (Malvern Panalytical). Mouse Glioma261 (GL261) or CT2A cells were plated in a 96 well plate at 10,000 cells per well. 24 hours later, cells were treated with transfected with lipofectamine + 3pRNA or lipofectamine + control RNA. 24 hours later, supernatants were collected for ELISA, and cells were stained for flow cytometry. The ELISA was conducted according to the manufacturer's protocol, and cells were stained for MHC I and run on a CellStream® Flow Cytometer (Cytek Biosciences). In vivo Experiments: Mice were inoculated with 1,000,000 GL261 or CT2A cells on the right flank. When tumors reached ~50 mm3, mice were treated intratumorally with PBS or RANs, with additional injections on days 3 and 6 post treatment initiation. Each treatment injection contained 10 µg of 3pRNA. Mice were euthanized and removed from the study when tumors reached a volume 1500 mm3, calculated as 0.5 x length x width2. Results, Discussion, and Conclusions: DLS showed that RANs were ~90 nm in diameter, and Ribogreen showed successful complexation of RNA to nanoparticles. We show that GL261 and CT2A cells treated in vitro with 3pRNA produce significantly more interferon beta (IFN-β) than mice treated with control RNA, but only CT2A cells increased MHC I expression following 3pRNA treatment. This lack of changes in GL261 cells is likely to high levels of MHC I expression at homeostasis, while the less immunogenic CT2A cells are activated by 3pRNA to express MHC I. Additionally, mice treated with RANs significantly delayed tumor growth (Fig. 1A) and prolonged survival in both GL261 and CT2A flank tumors (Fig. 1A). Specifically, RAN treatment of GL261 tumors extended the time to first death by 6 days with 40% of mice being long term survivors. While the impact of RANs were less pronounced in CT2A tumors, RANs significantly outperformed PBS and control RNA treated mice (Fig. 1B). Control RNA treated mice received the same mass of irrelevant RNA as 3pRNA in the same polymer as 3pRNA. Although the subcutaneous flank model of GBM does not fully represent the tumor microenvironment, our results still provide proof of concept that RANs can curtail GBM tumor growth. Our results show that we have successfully formulated nanoparticles that elicit a type one interferon response from GBM cells and can slow tumor growth. Future directions are optimizing the carrier for brain specific applications then moving to orthotopic models of GBM.

15A. NeuroGraph: Benchmarks for Graph Machine Learning in Brain Connectomics

Anwar Said

Machine learning provides a valuable tool for analyzing high-dimensional functional neuroimaging data, and is proving effective in predicting various neurological conditions, psychiatric disorders, and cognitive patterns. In functional Magnetic Resonance Imaging (MRI) research, interactions between brain regions are commonly modeled using graph-based representations. The potency of graph machine learning methods has been established across myriad domains, marking a transformative step in data interpretation and predictive modeling. Yet, despite their promise, the transposition of these techniques to the neuroimaging domain remains surprisingly under-explored due to the expansive preprocessing pipeline and large parameter search space for graph-based datasets construction. In this paper, we introduce NeuroGraph, a collection of graph-based neuroimaging datasets that span multiple categories of behavioral and cognitive traits. We delve deeply into the dataset generation search space by crafting 35 datasets within both static and dynamic contexts, running in excess of 15 baseline methods for benchmarking. Additionally, we provide generic frameworks for learning on dynamic as well as static graphs. Our extensive experiments lead to several key observations. Notably, using correlation vectors as node features, incorporating larger number of regions of interest, and employing sparser graphs lead to improved performance. To foster further advancements in graph-based data driven Neuroimaging, we offer a comprehensive open-source Python package that includes the datasets, baseline implementations, model training, and standard evaluation. The package is publicly accessible at https://anwar-said.github.io/anwarsaid/neurograph.html.

17A. Intramolecular interactions that stabilize factor XII in a closed form

Aleksandr Shamanaev

Background: In the absence of a contact surface, factor XII (FXII) is converted slowly to FXIIa by the protease kallikrein (PKa) because it is in a closed conformation that resists activation. Structure-function studies indicate that the FXII fibronectin type 2 (FN2) and kringle (KNG) domains are required for maintaining the closed structure. The artificial intelligence-based program AlphaFold predicts interactions between the FN2, KNG and catalytic (CD) domains that may stabilize the closed conformation. Aim: To test the importance of FXII intramolecular interactions predicted by AlphaFold. Methods: In the AlphaFold FXII structure, non-covalent interactions are predicted between Arg36 in FN2 and Glu502 in the CD, and Asp253 in KNG and Lys346 near the activation cleavage site. FXII with alanine substitutions for one of these four amino acids (FXII-R36A, FXII-E502A, FXII-D253K and FXII-K346A) were expressed in HEK293 cells. FXII-E502A was prone to autoproteolysis, so its active site serine was replaced to stabilize the zymogen (FXII-E502A,S544A). FXII variants with alanine substitutions for residues near amino acids 36, 253, 346 and 502 that were not predicted to be involved in intradomain interactions were prepared as controls. FXII activation was studied by chromogenic assay, and the effects of FXII variants on high-molecular-weight kininogen (HK) cleavage in plasma was studied by western blots. Results: FXII-R36A, FXII-D253K, FXII-K346A and FXII-E502A,S544A were activated by PKa substantially faster than FXII-WT or control FXII variants, indicating they are in open conformations. The addition of FXII-R36A, FXII-D253K and FXII-K346A to normal plasma caused rapid cleavage of HK, while FXII-WT did not, indicating the FXII variants induce rapid reciprocal activation with prekallikrein. Conclusion: Non-covalent interdomain interactions between Arg36 and Glu502, and between Asp253 and Lys346 are required to maintain FXII in a closed conformation when not surface bound. Our experimental data are in good agreement with the FXII structure predicted by AlphaFold.

Abstracts
Poster Presentations

19A. Activity dependent Clustering of Neuronal L-Type Calcium Channels by CaMKII
Qian Yang

Excitation-transcription (E-T) coupling, linking membrane depolarization to nuclear gene transcription, plays a critical role in regulating long-term synaptic modifications and is involved in learning and memory, as well as various diseases, including autism spectrum disorders (ASD), Alzheimer's disease, Huntington's disease, and epilepsy. Activation of L-type voltage-gated calcium channels (LTCCs) induces several forms of E-T coupling by increasing the local concentration of calcium ions within an LTCC nanodomain. Formation of LTCC/Ca2+ nanodomains may require clustering of the primary neuronal LTCC α1 subunits (CaV1.2 and CaV1.3). However, the molecular mechanism of LTCC clustering remains unknown. Here, we found that a neuronal depolarization that induces CREB Ser133 phosphorylation and c-fos expression also increases CaV1.3 LTCC clustering in cultured hippocampal neurons. Our previous work showed that binding of Ca2+/calmodulin-dependent protein kinase II (CaMKII) to an N-terminal RKR motif in CaV1.3 is required for LTCC-mediated E-T coupling. We coexpressed CaV1.3 containing two different epitope tags, with or without CaMKII in HEK cells. Co-immunoprecipitations (co-IPs) from the cell lysates revealed that CaMKII not only interacts with CaV1.3, but also assembles multimeric CaV1.3 LTCC complexes in an activity-dependent manner. Moreover, clustering of surface localized CaV1.3 α1 subunits in intact HEK293 cells was increased by pharmacological LTCC activation, but only in the presence of co-expressed wild-type CaMKII. Notably, the N-terminal CaMKII-binding RKR motif is conserved in CaV1.2, and CaMKII also facilitates the activity-dependent co-clustering of CaV1.3 and CaV1.2 in HEK293 cells. Furthermore, we found that beta2a auxiliary subunits, which also directly bind to CaMKII, facilitate CaMKII-dependent CaV1.2-CaV1.3 co-clustering, relative to the beta3 auxiliary subunit which lacks the ability to bind CaMKII. More interestingly, depolarization induced CaV1.2 or CaV1.3 LTCC clustering in cultured hippocampal neurons was disrupted by shRNA-knockdown of CaMKII expression. Our ongoing studies are examining the role of CaMKII in CaV1.2-CaV1.3 co-clustering in cultured neurons. Taken together, our work suggests that CaMKII mediates activity-dependent LTCC clustering, which may be crucial for initiating a specific long-range signal from LTCCs in the plasma membrane to the nucleus in various pathophysiological situations.

21A. Positive Allosteric Modulation of the M1 Muscarinic Acetylcholine Receptor via Tool Compound VU0486846 Prolongs Survival and Improves Cognition in Neurodegenerative Diseases
Daniel Schultz

Prion and prion-like neurodegenerative diseases are devastating afflictions that impact millions of people worldwide. In the US, roughly 6.7 million persons (1 in 9) above age 65 exhibit Alzheimer's dementia and nearly 1 million people across all age groups exhibit Parkinson's disease. Treatments to slow or stop the progression of these and similar diseases are currently lacking, prompting significant research efforts in academia and industry. To this end, we have developed the tool compound VU0486846, a positive allosteric modulator (PAM) of the M1 subtype of the muscarinic acetylcholine receptor (mAChR) G protein-coupled receptor (GPCR) family. This receptor subtype is highly expressed within the central nervous system (CNS) and, to a lesser extent, within the periphery, and is implicated in the regulation of cognitive and behavioral processes. Through extensive medicinal chemistry efforts, VU0486846 has been identified as a brain-penetrant, selective M1 PAM with a favorable drug metabolism and pharmacokinetic (DMPK) profile and no overlap with the orthosteric acetylcholine binding site. This valuable tool compound exhibits procognitive activity in murine in vivo models while simultaneously displaying no adverse agonism- or cholinergic toxicity-related liabilities. Furthermore, administration of VU0486846 prolonged survival and improved the associated molecular marker profile in prion disease mouse models.

23A. Feasibility of Systemic Radiotracer for Pre-operative Staging and Sentinel Lymph Node Biopsy in Head and Neck Cancer
Nicole Meeks

Background: In patients diagnosed with head and neck squamous cell carcinoma (HNSCC), the presence of lymph node metastasis greatly reduces the 5-year survival regardless of the primary tumor T stage. Sentinel lymph node biopsy is an accepted mechanism of nodal assessment in patients diagnosed with oral cavity squamous cell carcinoma, but has not been adopted in the United States for a range of reasons such as patient tolerance, variability in tumor injection techniques, and lack of intra-operative staging. Therefore detection of regional nodal metastasis has been an elective neck dissection, which is associated with morbidity including shoulder dysfunction, lymphedema, and scarring. The aim of this study is to determine whether systemic administration of 111In-panitumumab is safe and can be used for detection of sentinel lymph nodes on pre-operative imaging and intra-operatively. Objective: The primary objective of this study is to examine the safety of 111In-Panitumumab in patients diagnosed with HNSCC as defined by the number of CTCAE v5 Grade 2 or higher adverse events by day 15 after infusion. The secondary objectives are to determine if 111In-panitumumab can detect lymph nodes on pre-operative imaging, as well as the feasibility, sensitivity, and specificity of identifying sentinel lymph nodes via systemic injection of 111In-panitumumab compared to conventional local injection with an optical dye at the time of surgery. Methods: This is an ongoing phase 1, open-label, non-randomized study approved by the FDA, Vanderbilt IRB, and Stanford IRB committees. Patients presenting to Head and Neck Oncology clinic diagnosed with any T site and stage of head and neck squamous cell carcinoma undergoing resection and neck dissection were screened for inclusion. Exclusion criteria include history of myocardial infarction, cerebrovascular accident, infusion reaction to monoclonal antibodies, pregnancy, and abnormal kidney function determine by eGFR and serum creatinine. Enrolled subjects received an IV loading dose of 50mg unlabeled panitumumab followed by an IV bolus of 5mCi (⍰ 20%) of 111In-panitumumab 1 to 5 days prior to surgery. After receiving the study drug, subjects underwent SPECT/CT head and neck imaging. Intraoperatively, patients underwent peritumoral injection with indocyanine green (ICG) followed by conventional sentinel lymph node mapping. Gamma tracing was performed to evaluate the number of 111In-Pan lymph nodes detectable by gamma counting in situ. A standard of care neck dissection was performed with ex vivo quantification of gamma signal.

Specimens were sent via routine histopathology for pathologic assessment. Subjects were followed for 15 days after infusion. Results: Four patients have been enrolled and completed the study at Stanford. All four patients had significant uptake of the radiotracer within the primary and visualization of upper echelon lymph nodes on SPECT/CT imaging. One patient who did not have a sentinel node identified by ICG, however, had the highest gamma counts in the expected drainage basin based on primary tumor location. Two of the four patients had a positive sentinel node determined by pathology, of which positively correlated with the radiotracer. None of the patients had an identifiable adverse reaction attributed to the study drug. Conclusions: In the initial subjects of this ongoing study, 111In-panitumumab appears safe and feasible for pre-operative SPECT/CT imaging and intra-operative detection of lymph nodes via gamma tracing.

25A. Hepatic specific Cholesteryl Ester Transfer Protein regulates Metabolic Associated Fatty Liver Disease by sex dimorphism
Sivaprakasam Chinnarasu

Significance: Cholesteryl Ester Transfer Protein (CETP) is a lipid transfer protein expressed in the liver and adipose in humans which shuttles triglycerides and cholesteryl esters between the lipoproteins. Metabolic Associated fatty liver disease (MAFLD) is a wide spectrum of disease from simple steatosis to steatohepatitis and hepatocellular cancer, which remains without effective therapies and no FDA approval drugs available. There are male-female sex differences in the pathophysiology of MAFLD and the associated dyslipidemia that gives rise to cardiovascular risk. Understanding mechanisms of sex differences in MAFLD and lipoprotein metabolism may yield novel therapeutic targets. However, the role of CETP in sex associated risks of MAFLD has not been well defined. Approach: Mice naturally lack CETP and thus transgenic approaches can be used as a model to define the contribution of CETP toward dyslipidemia and MAFLD. We used both mice transgenic for the human CETP gene regulated by its natural flanking sequences (huCETP) and a liver-targeted CETPexpressing adeno-associated virus (AAV8-TBG-(GFP/CETP), here termed hAAV-CETP) injected mice models to achieve our goals. Results: We identified that in both models CETP has sex-specific effects on dyslipidemia and MAFLD. High-fat diet (HFD) fed mice increased body weight and adiposity in both female and male mice regardless of CETP expression. In male hAAV-CETP mice liver weight increased, and glucose tolerance worsened compared to hAAV-GFP control. In female hAAV-CETP mice, glucose tolerance was improved consistent with our prior clamp results in huCETP mice. In male mice hAAV-CETP expression resulted increased oil-red-O staining and more lipid droplet and accumulation compared to both hAAV-GFP and female hAAV-CETP groups. We found in male mice hAAV-CETP worsened steps in hepatic lipid metabolism, while CETP improved steps in hepatic lipid metabolism in females (Acc, Ldlr, Mttp and Dgat1). Similarly, glucose metabolism genes (Pepck and G6pc) were upregulated by CETP male mice and downregulated by CETP female mice. Liver fibrosis induced genes mRNA expression levels upregulated on male CETP but no changes on female mice. We performed liver mRNA sequencing from huCETP mice that underwent orchiectomy and testosterone treatment. We found that approximately 1500 genes differentially expressed by the presence of CETP in the male liver. Most of these were androgen-dependent. Conclusion: Our studies support a role of CETP expression with regard to sex-specific risk of MAFLD and dyslipidemia. This may suggest that CETP could be target to improve MAFLD in males and may facilitate sex-specific precision medicine.

27A. Prediction Models for Incidence Tuberculosis in Contacts of People with Tuberculosis: A Systematic Review
María B. Arriaga

Background: Around of 5–10% individuals infected with M. tuberculosis (MTB) develop active TB, with 50% developing active disease within 2 years after infection. Therefore, the management (tracing and evaluation) of TB close contacts is important for the overall control of TB Identification and evaluation of predictive models for TB incidence in contacts of pulmonary TB cases would help adjust the structure of prediction models and thereby improve prognosis for TB disease. Methods: A systematic search was performed in data sources of PubMed, Embase, Scopus and Web of Science of studies published between 1980 - 2022 in the English, Portuguese, and Spanish languages. Articles that developed predictive models for the incidence of pulmonary TB among TB contacts (any definition) were included. The Prediction model Risk of Bias Assessment Tool was used for quality assessment and the CHARMS (Critical Appraisal and Data Extraction for Systematic Reviews of Prediction Modelling Studies) checklist was used for data extraction. The study was registered on the international prospective register of systematic reviews PROSPERO (CRD42022377902). Results: From 5,397 articles identified, 196 were full-text articles evaluated and 40 were included for data extraction. We obtained 53 prediction models. The definition of contact was varied between studies, considering the number of hours of exposure and the relationship of the contact with the TB index case. Only eight studies informed internal or external validation of prediction model performed. Characteristics of TB contacts such as age, sex, TB skin test, TB preventive treatment, nutrition status, previous TB, BCG scar and type of contact and, characteristic of TB index cases such as sputum smear, age, cavities on X-ray and sex were the most common predictors. Due to the heterogeneity of the contact definitions, high risk of bias in the analyzes including the lack of validation of models between the studies, it was not possible to perform a meta-analysis. Conclusion: The prediction models existing of TB incidence in TB contacts are poorly reported and validated and the absence of standard definition for contact renders the results useless for clinical decision. Studies are needed that develop predictive models following standardized guidelines.

29A. Transition metals alloys trigger blood coagulation via intrinsic pathway: implications for intravascular devices
Maxim Litvak

Introduction. Transition metals and their alloys, such as medical grade stainless steel, titanium and tantalum alloys have well-established roles in manufacturing medical devices and implants because of their strength and resistance to corrosion. These materials are generally considered "hemocompatible" because they have relatively limited capacities to trigger blood host-defense responses. However, a growing body of evidence

indicates that transition metals and their alloys promote blood coagulation. Patients, implanted with intravascular devices, made of titanium (left ventricular assist devices, artificial valves) or stainless steel (artificial valves, percutaneously implantable heart pumps) always require extensive anticoagulation and antiplatelet therapy contrast to biological valve and heart transplants. Although the role of platelet adhesion and activation on artificial surfaces is undoubtedly important, antiplatelet therapy alone cannot prevent all possible thrombotic complications, which necessitates prescription of Vitamin K antagonists resulting in high rate of bleeding complications. The contact system, comprised of intrinsic pathway clotting factors prekallikrein (PK), factor XII (FXII), factor XI (FXI) and the cofactor/substrate high molecular-weight kininogen (HK), evolutionary intended to recognize foreign surfaces very first, has recently been identified as an important pharmacological target for safer anticoagulation. The aims of the study were to determine thrombogenic potential of internal metallic surfaces of intravascular devices; compare the most common compounds as titanium (Ti), tantalum (Ta) and stainless steel (SS) with known contact activators (kaolin) and non-transition metal (aluminum) for their capacities to induce plasma coagulation via intrinsic pathway; to evaluate binding/activation of contact factors and effects of contact activation inhibitors. Materials and Methods. Recalcification clotting times (RCTs) were measured directly during incubation (37°C) of pooled normal plasma (PNP) on the internal surfaces of Left Ventricular Assist Device (LVAD HeartWare, Framingham, MA) and Implantable Heart Pump (Impella Abiomed, Danvers, MA) with visual detection. Clotting assays in PNP and plasmas deficient in factor XII, prekallikrein, or high-molecular-weight kininogen, chromogenic substrate assays with purified plasma contact proteins (FXII, PK, HK) and pull-down experiments were performed, using as contact activators kaolin and nano- and microparticles made of titanium (70nm), tantalum (50nm), aluminum (70nm) and stainless steel 316 (5um). Samples of plasma incubated with powders for various times underwent centrifugation for 1 minute, 14000g. Supernatants and pellets were separately fractionated by nonreducing SDS-PAGE and transferred to nitrocellulose. Blots were probed with HRPconjugated polyclonal IgG to different clotting factors and detected by chemiluminescence. Results. Plasma RCTs were significantly ($p<0.05$) shortened during incubation on the titanium surfaces of LVAD (4.5±0.7min) and steel surfaces of Impella device(8.9±0.8min) compared to polypropylene (13.9±0.8min). PNP clotting times measured with equivalent surface amounts of titanium (103.1±7.8s), tantalum (118.3±1.8s) and stainless-steel (127.1±6.9s) powders were comparable to kaolin (108.6±1.4s) and were significantly ($p<0.05$) reduced compared controls (328.4±19.2s) and aluminum (304.8±12.5s). Chromogenic substrate assays and Coomassie-stained SDS PAGE demonstrated that Titanium quickly facilitated purified plasma FXII autoactivation in buffered solution, while Tantalum and Stainless steel showed significantly slower rate of FXII autoactivation. Autoactivation FXII on Aluminum was negligible. Titanium expectedly facilitated FXII-PK reciprocal activation, while Tantalum and Stainless steel required presence of HK in the solution. Titanium, which carry a negative charge in physiologic conditions, contrast to Aluminum (positively charged) rapidly bind FXII, prekallikrein and HK in plasma, inducing reciprocal activation and HK cleavage. Anti-FXII antibodies, small molecule kallikrein inhibitor KV999372 or coating surface with polyarginine inhibited FXII activation on Titanium, reduced kallikrein generation and HK cleavage. Conclusions: corrosion-resistant transition metals and their alloys commonly employed in biomedical applications are potent contact pathway activators, although the mechanisms underlying their effect differs between particular metals. Disrupting negative surface charge with positive polypeptides' coating or use of intrinsic pathway proteases inhibitors may help to mitigate prothrombotic and proinflammatory consequences of contact activation in patients with intravascular devices.

31A. Uncertainty quantification in microstructure images with moment invariants

Arulmurugan Senthilnathan

The performance of an additively manufactured part/component depends on their material properties which are heavily influenced by the microstructure. However, variability in the manufacturing process affects the microstructure. The Electron Back Scattering Diffraction (EBSD) imaging technique is employed to study the microstructure and generates a topological map characterizing the features (e.g., grain shape, grain size and orientation) of a microstructure in terms of pixel intensity values. Uncertainties from various sources during experiments and simulations are propagated onto the pixel intensity values of the microstructure image. However, the high computation cost to study the microstructure images of large dimensions necessitates the development of a reversible reduced dimensional space to study the uncertainty. Therefore, the statistical concept of moment invariants is utilized for reducing the image dimensions and for uncertainty quantification. The developed technique paves the way for solving stochastic optimization problems for optimal process design and is universally applicable to any kind of image.

33A. Size and Stiffness Based Microfluidic Sorting of Metastatic Breast Cancer Cells to Examine Mechanotype Stability and Heritability

Katie Young

While the metastatic and migratory potential of tumor cells is related to their mechanical properties, previous studies of cell stiffness have been limited to observing cell mechanics as an effect of rather than a potential driving force of metastasis. To explore this potential causal link, I first separated stiff and soft MDA-MB-231 breast cancer cell subpopulations with a microfluidic stiffness-based cell sorting device (Figure 1a). This technology consists of a microchannel with multiple diagonal ridges that hang down from the top plane of the device that compress cells as they flow through the 8 micron gap (Figure 1b). Cells that are either highly deformable, smaller, more viscous, or less adhesive are able to squeeze under the ridges and follow the hydrodynamic forces of the flowing buffer around the cells to travel towards a specific device outlet. Alternatively, cells that are stiffer, larger, less viscous, or more adhesive resist compression and are moved by the diagonal ridges perpendicular to the fluid flow toward different device outlets (Figure 1c). In this way, a heterogenous population of cells can be sorted into subpopulations with different mechanical properties. For the first time with this device design, staged sorting was used to first sort cells by size and then by stiffness. Atomic force microscopy (AFM) and micropipette aspiration were used to compare the stiffness of cells deflected to the soft and stiff outlets, resulting in an observed

enrichment of stiff cells. After fluorescently labeling each subpopulation, the cells were re-sorted and flow cytometry was used to identify whether the labeled cells initially sorted into the stiff or soft subpopulations re-sort into the same stiff or soft subsets following cell division. The stability and heritability of cancer cells was also investigated by collecting AFM stiffness measurements of the same single cells over time. Understanding cell mechanotype as a transient state or an inherent property gives us insight into the plasticity of cancer cells' mechanical state, which can eventually lead to the development of targeted therapies to slow or stop metastasis through the modulation of cancer cell mechanics.

35A. Occupational benzene exposure and cancer risk among Chinese men: A report from the Shanghai Men's Health Study
Douglas DeMoulin

Objective: To assess the associations of occupational exposure to benzene with the risk of cancers of lung, liver, kidney, stomach, myeloma, leukemia and lymphoma. Methods: This study used data collected on the baseline survey of the Shanghai Men's Health Study, a population-based cohort study of 61,377 men aged 40-74 years, enrolled between 2002-2006 and followed for cancer incidence through 2016. Job-exposure matrices (JEM), constructed by industrial hygienists specifically for the study population, were used to estimate job-related benzene exposure intensity and industry's probability of exposure to benzene based on longest job held. Multivariable cox regression analyses were performed to estimate hazard ratios (HR) and 95% confidence intervals (CI) for the cancers of interest in association with occupational exposure to benzene with adjustment for demographic characteristics and known risk factors, including cigarette smoking and alcohol consumption. Results: Over 15 years of follow-up, a total of 1,145 lung, 656 stomach, 445 liver, 243 kidney cancer cases, and 224 leukemia and lymphoma, and 46 myeloma cases were identified in the cohort. The longest held jobs with high intensity of benzene exposure was significantly associated with increased risk of lung cancer (HR=1.5, 95%CI=1.1-2.0), stomach cancer (HR=1.5, 95%CI=1.1-2.0) as well as leukemia and lymphoma (HR=2.0, 95%CI=1.1-3.8) compared to these without benzene exposure. Significant associations were also observed for adenocarcinoma of lungs (HR=1.9, 95%CI=1.1-3.2) and stomach (HR=1.3, 95%CI=1.0-1.8). Similar patterns were observed when cumulative benzene exposure from all jobs and industrial based exposure assessment are considered. Cumulative exposure to >550mg/m3 benzene was associated with elevated leukemia and lymphoma risk only among alcohol drinkers (HR=4.4, 95%CI=2.1-9.2) and never smokers (HR=2.8, 95%CI=1.4-5.4). Tests for multiplicative interactions were both significant. Occupational exposure to benzene exposure was not significantly associated with risk of liver and kidney cancers as well as myeloma. Conclusion: High intensity of occupational exposure to benzene assessed by JEM was associated with a 1.3 to 2.0-fold increased risk of stomach cancer, lung cancer and, leukemia and lymphoma among Chinese men. Alcohol drink and smoking modify the association of benzene exposure with leukemia and lymphoma risk.

37A. The Maya are a People of Movement: An Isotopic Assessment at Chactemal (Santa Rita Corozal), Northern Belize
Angelina J. Locker

Nestled between the Rio Hondo and New River in Corozal District northern Belize and situated within the border zone between the Northern and Southern Lowlands, the coastal Maya archaeological site of Santa Rita Corozal, hereafter Chactemal, was continuously occupied from the Middle Preclassic (BCE 800–300) through the Late Postclassic (CE 1250–1531). While many sites in the Southern Lowlands experienced decline and abandonment in the Terminal Classic (CE 800–900), Chactemal flourished, reaching its apex in the Late Postclassic when it rose to regional prominence to become the capital of the Chetumal Province. It is not well-understood how mobility influenced the population growth Chactemal experienced. We measured stable oxygen isotopes of dental enamel (n=108 samples) and bone carbonate (n=96 samples) from 100 Ancestors recovered from Chactemal to diachronically assess movement. Approval for isotopic research was granted by the Belize Institute of Archaeology. Additionally, we co-developed this work alongside local Maya organizations and villages in Corozal District. δ18O values (mean= – 4.0 ‰ VPDB, SD= 1.4, range= – 7.6 ‰ to – 0.8 ‰ VPDB) indicate non-local Ancestors are present within the burial population and suggest non-local Ancestors from the Preclassic came from different places than those in the Late Postclassic. We present evidence to suggest that Chactemal's geographic positioning on the coast, between two rivers, and within the border zone between the Northern and Southern Lowlands attracted people from other places throughout time.

39A. Unraveling the genetics underlying the brain function of the rhythm network
Yasmina Mekki

Background Understanding genetically associated brain individual differences underlying the human capacity to perceive and synchronize to musical rhythm will provide insights into its neural mechanisms. Prior studies linked genetic variation to the ability to move in time with a musical beat and revealed a complex, and polygenic genetic architecture underlying human rhythm. At the brain level, its genetic architecture remains largely unknown. Neural activity measured during task performance is the standard approach to study rhythm processing. However, a growing body of evidence suggests that there is a close correspondence between resting state networks and known cognitive task activation maps (smith et al., 2009, Cole et al., 2014, Tavor et al., 2016). Our aim is to take advantage of resting-state functional MRI data to understand how the brain supports rhythm by unraveling the genetic factors that might contribute to it. Methods We used individuals from the UK Biobank cohort with both resting-state functional MRI and genotyping data. We excluded participants with unusual heterozygosity, high missingness, and sex mismatches. We further restricted our analyses to individuals with white British ancestry in order to avoid any possible confounding effects related to ancestry. This resulted in 31,768 individuals (mean age = 55.31, 16,507 females) passing the sample QC Using PLINK v1.9, we excluded variants with minor allele frequency

< 0.01, and imputation quality INFO scores < 0.8. Multiallelic variants were also removed. 53 Regions of interest (ROIs) were defined as the intersection between rhythm networks (informed by Kasdan et al. 2022) and the combination of parcellations from AICHA and Diedrichsen cerebellar atlases. We constructed a rhythm functional connectome for each individual using a shrunk estimate of partial correlation between each pair of the defined ROIs, resulting in 1,378 functional connectivities (FCs) for each individual. These FCs were pre-residualised controlling for covariates including sex, genotype array type, age, recruitment site, and first ten genetic principal components, then normalized using a rank-based inverse-normal transformation. We estimated the SNP-based heritability of the FCs using GCTA (v1.93.0beta) and performed a multivariate genome-wide association study (mGWAS) using MOSTest (Van der meer et al., 2020). Results SNP-based heritability analysis showed that 146 out of the 1,378 FCs are heritable (pFDR<0.05). We investigated which genetic variants contribute to the heritable rhythm-related FCs by performing a mGWAS. There were 22 significant loci (genomic threshold p<5e-8) associated with different aspects of the rhythm network. We investigated the shared genetic underlying both brain rhythm network mGWAS and behavioral rhythm GWAS (Niarchou et al., 2022) and found a significant genetic correlation (ρ=0.18, se=±0.05, p=1.93e-14). An extensive functional annotation performed highlighted a significant functional enrichment of genes involved in embryonic brain expression. Conclusions This preliminary work represents a step forward towards understanding how genes influence the neurofunctional basis of human rhythm skills, complementing behavioral results. By using resting-state fMRI data, we tried to contribute to alternative task-free approaches to study behavioral traits such as rhythm and its genetic underpinnings.

41A. Type 2 diabetes mellitus, its type and blood pressure traits: A two-sample Mendelian randomization study

Til B. Basnet

Diabetes and hypertension are common co-morbidities and are often related to each other. Type 2 diabetes mellitus (T2DM) is potentially linked with hypertension via hyperinsulinemia caused by insulin resistance (IR). The present research finds the causal association of T2DM types with hypertension using genetic variants as a proxy in Mendelian randomization (MR) techniques. We clumped statistically significant (P-value <5x10-8) uncorrelated (R2 <0.01) single nucleotide variants (SNVs) from published GWAS as genetic instruments for T2DM and its type (N-SNVs: 237 for T2DM, 60 for insulin deficiency (ID) T2DM, and 63 for IR-T2DM). Summary statistics for the same SNVs for blood pressure (BP) traits were generated with a regression model in 757601 European individuals. We used inverse variance weighted (IVW) random-effects analysis as the primary analysis, followed by MR-Egger, MR-mode, MR-weighted median, and multivariable MR as sensitivity analyses. As a positive control, we performed MR analyses with body mass index as exposure for BP traits. Genetically predicted T2DM was associated with an increased risk of higher BP (SBP: β, 0.711; 95% CI, 0.485 – 0.937; P = <0.001; DBP: β, 0.192; 95% CI, 0.047 – 0.337; P = 0.01; PP: β, 0.566; 95% CI, 0.430 – 0.703; P < 0.001) in IVW analysis. Upon extracting the T2DM type SNVs, genetically predisposed ID-T2DM had SBP, DBP, and PP that are 0.532, 0.019, and 0.489 mmHg higher than non-ID-T2DM in IVW analysis. Likewise, the presence of IR-T2DM was associated with an average increase of 1.79, 0.703, and 1.126 mmHg in SBP, DBP, and PP respectively. These findings were also supported by sensitivity analysis. Evidence guided by instrumental genetic variables shows that T2DM is causally associated with higher BP, specifically SBP and PP. Moreover, the IR-T2DM type has a greater impact on increased BP, mechanistically supporting insulin resistance leads to increased BP.

43A. Assessing the glycation effect and mechanical damage in human cortical bone through Raman Spectroscopy

Rafay Ahmed

Bone has complex hierarchical structure composed of mineral, collagen, lipids, water, and non-collagenous proteins. Bone mineral gives hardness whereas collagen provides tensile strength and flexibility. Being able to probe at the ultrastructural level of bone hierarchy is important to understand age- and disease-related changes in the fracture resistance. Raman spectroscopy (RS) probes molecular vibration and is sensitive to advanced glycation end-products, damage to the bone matrix, thus fracture toughness properties. We studied effect of glycation and mechanical damage on characteristics of the Amide I Band. N=20 cadaveric femurs were obtained from Vanderbilt Cadaver Program. We extracted medial and lateral quadrants of cortical bone (~50 mm) along the longitudinal axis of the mid-shaft using a saw. Dog-bone specimens' gauge region (10 × 2 × 2 mm) were created for tensile tests while 2-rectangular beams (50 × 4 × 3 mm) for glycation incubation. A) For tensile tests, specimens were pulled-to-failure at 5mm/min using 1000 N load cell. RS was acquired through gauge region (GR) before and after tests. B) For glycation, beam-1 (control) was incubated in 50 mM sodium phosphate buffer, 0.02% sodium azide, protease inhibitor cocktail, pH 7.6 and beam-2 (Glucose) with same buffer plus 0.5 M glucose for 5-weeks at 45 0C. RS was acquired through 20 glycated, 20 control specimens before and after incubation. RS results indicate that Amide I sub-peak ratio 1670/1640 significantly increased post tensile tests compared to baseline. 1670 and 1640 cm-1 peaks are associated with random coils and alpha helix respectively. Thus, more disorganized structures are formed because of tensile damages. Glycated beams show lower 1670/1640 ratio compared to baseline and control. This in part due to increase in packing density of collagen molecules upon glycation. Overall, our result indicate the RS can assess cortical damage and sugar-mediated changes in the amide I band.

Abstracts
Poster Presentations

45A. Targeted Temperature Cooling or Rewarming for Porcine Hearts Procured After Donation After Circulatory Death
Timothy R. Harris

Background: Primary graft dysfunction (PGD) occurs about 10% of heart transplant patients and is associated with significant mortality. One well-known contributor to PGD is prolonged cold ischemic time between induction of cardiac arrest and reperfusion. As such, current practice limits cold ischemic time to less than 4 hours. Heart allografts are typically stored on ice between procurement and reperfusion (0oC), however, recent studies of lung allografts stored at 10oC demonstrate prolonged storage viability with decreased ischemia-reperfusion injury. Our efforts are to identify a temperature for static heart storage that allows for prolonged storage with less ischemia-reperfusion injury. Essential to achieving internal validity is to ensure homogenous cooling of cardiac tissue to a desired temperature. The aim of this study is to design a mechanism for targeted temperature cooling for porcine hearts at various temperatures. Methods: Using a circulatory arrest model, heart allografts from Yorkshire-Landrace pigs (N=4) were procured using standard operative technique. Hearts were preserved with cold University of WisconsinTM cardioplegia and explanted. Hearts were then placed in a NIST-verified refrigerator or cooler, and tissue temperature was recorded using forward looking infrared thermography as well as myocardial temperature probes at the interventricular septum every 15 minutes. A cooling curve was created and time to cool tissue to a desired temperature (0oC, 4oC, 10oC, or 18oC) was recorded as primary outputs. Results: Porcine heart stored on ice was able to achieve 0oC at 75 minutes. Average normalized cardiac mass was 4.69g/kg + 0.24kg. A heart stored at 4oC achieved goal temperature at 105 minutes, while heart stored at 10oC achieved a myocardial temperature of 10.5oC by 180 minutes. Heart stored at 18oC achieved 17.5oC by 240 minutes. Thermography demonstrated qualitative homogeneous desired temperature that was preserved at 4 and 8 hours for all groups. Conclusion: We have demonstrated that that porcine hearts are able to be cooled to a desired set temperature within 1oC by 4 hours. Interestingly, hearts stored in colder ambient environments achieve desired temperature faster than hearts stored at warmer temperatures. This may be due to a larger heat gradient contributing to faster cooling. Further assessment of tissue cooling as well as re-warming to normothermia is warranted to translate these studies into clinical practice.

47A. Drug repurposing for Alzheimer's disease: the use of genetics-enriched, neuropathology-associated SPI1 regulon in microglia
Yuting Tan

Alzheimer's disease (AD) is characterized by progressive decline in memory and cognition and involves multiple brain cell types. Among them, microglia play a crucial role. Evidence accumulates suggesting drugs with support from genetics are more likely to succeed to the market. Here, we aim to identify genetics-enriched, AD-relevant regulatory programs in microglia to guide the search of approved drugs for repurposing toward AD. We detected regulons from scRNAseq data, with some of them being significantly enriched in AD heritability. Most of these genetics-enriched regulons are active in microglia, and the SPI1-regulon ranked with the highest AD heritability. By evaluating the proximity between drug target(s) and SPI1-regulon genes, we identified several promising candidate drugs for AD. In conclusion, we showed combining scRNAseq, GWAS summary statistics and neuropathological traits of AD enabled the dissection of genetics-enriched, AD-relevant regulatory programs in human microglia, which have value in guiding the drug purposing for AD.

49A. Polarization sensitive Raman spectroscopic studies for rattail tendon tissue.
Chitra Shaji

Raman spectroscopy is an effective tool for studying the chemical composition of materials, that is widely used for various biomedical applications. We have combined the polarization of light with the Raman spectroscopic technique to extract more information about structural orientations of molecules along with the biochemical properties of the sample. The rattail tendon being highly rich in collagen, is studied extensively using polarization-sensitive Raman spectroscopy via an incident laser whose states of polarization are varied and by assessing the Raman scattered light with horizontal and vertical polarization analysers. A clear change in the peak corresponding to the collagen molecule of rattail tendon is observed as the incident state of polarization is varied, with and without polarization analysis of the Raman scattered light. These extensive studies for polarization Raman spectroscopy using a known, highly collagenous structure, are essential for standardizing the technique.

Abstracts
Poster Presentations

Poster Session B

2B. Advancing the Construction of High Spatial Resolution Multimodal Molecular Atlases with the Aid of Data-Driven Image Fusion
Olof Gerdur Isberg

Introduction: Matrix-assisted laser desorption/ionization imaging mass spectrometry (MALDI IMS) enables the untargeted, highly multiplexed mapping of a wide range of biomolecules, such as small metabolites, lipids, and proteins in situ. However, limitations in throughput and spatial resolution make performing MALDI IMS impractical for applications that require more than a few million pixels – e.g., high spatial resolution whole slide imaging (WSI) and 3-dimensional (3-D) molecular imaging. Herein, we assess the potential for data-driven image fusion to aid in advancing these two challenging application areas by providing predictions to complement classical ion measurements. By registering and fusing IMS and complimentary microscopy modalities, we aim to develop practical sampling methods that allow for robust ion distribution predictions across WSIs as well as 3-D volumes. Methods: Human kidney tissue was cryosectioned at a 10-µm thickness and thaw mounted onto indium tin-oxide (ITO) coated glass slides. Autofluorescence microscopy (AF) images were acquired using EGFP, DAPI, and DsRed filters on a Zeiss AxioScan Z1slide scanner prior to MALDI matrix application. Samples were sublimated with a 2.5 mg/mL solution an aminated cinnamic acid analog. MALDI IMS was performed from m/z 300 to 1600 on a Prototype Bruker timsTOF Pro (Q-TOF) MS system (BrukerDaltonics, Bremen, Germany) in positive and negative ion modes. The images were collected with a 10 µm pixel size with 100 laser shots per pixel at 35% laser energy. Ion image data was visualized using SCiLS Lab Version 2023 and subsequently processed using an in-house processing pipeline. Preliminary Data: A mock 3-D data set was collected to assess data-driven image fusion for out-of-sample prediction across serial human kidney whole slide images. All cryosections were collected with 10-µm thickness. Sets of 3 consecutive sections were collected for every 20 sections cut. Five 3-section sets were collected in total, with the first set including sections 1, 2, and 3, the second set including sections number 21, 22, and 23, and so on. For each set, every section was analyzed using AF microscopy to enable automated segmentation of nephron substructures using previously developed tools. The first section in each set was then analyzed using IMS in positive ion mode. A rectangular measurement region was analyzed with 10-µm pixel size resulting in ~1.2 million pixels, ensuring that all kidney structures were sampled (e.g., cortex, medulla, and vasculature). A similar analysis was performed on the third section of each set but in negative ion mode. These data are used to construct posIMS-AF and negIMS-AF fusion models in-section between MALDI IMS and AF/stained microscopy measurements, using in-house tools (http://fusion.vueinnovations.com/). These enable certain positive and negative mode ion species to be predicted on the basis of microscopy in the second tissue section of each 3-set, both at 10-µm and 5-µm pixel sizes. To assess ion distribution prediction, ground-truth IMS measurements were also collected on the second tissue section. Multiple measurement regions were collected from the medulla and cortex with both 10-µm and 5-µm pixel sizes, for both positive and negative ion modes. This approach was repeated on all five sets of tissue sections, after which all samples were stained with Periodic acid-Schiff (PAS) and imaged with brightfield microscopy. Fusion performance is assessed across all detected ions. These experiments will inform intelligent sampling methods to leverage data-driven image fusion to make large-scale 3-D tissue mapping more practical. Abstract Novelty: We investigate and evaluate how out-of-sample prediction based on data-driven image fusion can advance high-spatial-resolution IMS across 3-D tissue volumes. Abstract Preliminary Data: Out-of-sample IMS prediction of several known lipids from 5µm-pixel size to 1-µm resolution based on co-registered stained microscopy.

4B. Whole Foods for Prediabetes: Feasibility and Acceptability of a Dietary Guidelines-Based Intervention for Type 2 Diabetes Prevention in Families
Nadia M. Sneed

Background: Diet patterns (e.g., Mediterranean) rich in whole foods (e.g., fruits, vegetables, etc.) can improve diabetes outcomes (e.g., HbA1c), but are difficult to maintain long-term. A family-centered whole foods diet pattern adapted from the 2020-2025 Dietary Guidelines for Americans (DGA) may be an alternative solution to treat prediabetes but has not been tested in adults. Methods: A 2-week single-arm pre-post experimental controlled-feeding study of a whole foods diet adapted from the 2020-2025 DGA was conducted for adults (25-59 years) with prediabetes and their biological offspring (6-17 years). Participants received 2 weeks of menus/grocery delivery, and weekly counseling by a registered dietitian. Feasibility was based on having a ≥50% family retention rate and ≥80% completion of outcome measures including adult-child anthropometrics (weight [kg], height [cm], body mass index [BMI] including BMI% and Zscores for offspring, and waist circumference [cm]) and child diet quality estimated using the Healthy Eating Index (HEI-2020) from a random 14-day food diary entry. Acceptability was assessed during an optional focus-group session. Paired (dependent sample) t-tests were used to compare differences between baseline and 2-week anthropometrics measures, and child HEI- 2020 total and sub-scores. Qualitative data were analyzed using thematic analysis to assess diet satisfaction and barriers and facilitators of diet adherence. Results: Eight families enrolled (n=8 adults, n=12 offspring), and 7 families completed the study (12% attrition) including 100% of outcome measures. Adult participants maintained a stable weight (within ~6% body weight) from baseline to follow-up (83.2 to 79.8 kg/m2, median difference -3.4 kg/m2). Offspring demonstrated a significant 24-point increase in 2015-HEI diet quality scores (median difference of 50 to 74; p=.01). Focus group participants (n=4 adults) reported being satisfied with the program and expressed a willingness to continue the protocol despite identified barriers. Conclusions: Findings from this study suggest that a whole foods diet is a feasible and acceptable intervention for high-risk for T2D families.

6B. Reduced GABA Uptake and Altered GABAergic Neurotransmission in Slc6a1S295L Knock-In Mouse Associated with Epileptic Encephalopathy
Kirill Zavalin

Rationale: The S295L mutant variant of SLC6A1, encoding γ-aminobutyric acid (GABA) transporter 1 (GAT-1), is associated with developmental and epileptic encephalopathy (DEE) in human patients. DEEs encapsulate debilitating disorders marked by interrelated phenotypes of epilepsy and developmental delay, for which pathophysiologies are often poorly defined, and treatment options are lacking, requiring urgent investigation of both. Previously, we demonstrated that GAT-1(S295L) has diminished expression and ability to transport GABA in vitro. Moreover, we showed reduced GABA uptake in synaptosomes and reduced GAT-1 expression in brain tissue of Slc6a1S295L knock-in mice, which recapitulate the DEE phenotype observed in human patients. Based on these results, we hypothesize that the core pathologic dysfunction in SLC6A1(S295L) patients is reduced GABA uptake and associated changes in GABAergic neurotransmission. To test this hypothesis, we investigated pathologic changes in GABA uptake, and tonic and synaptic GABAergic events ex vivo in Slc6a1S295L mice. Methods: Male and female Slc6a1+/S295L mice (Shanghai Model Organisms, NM-KI-190014) in C57BL/6J background were used. Acute ex vivo brain slices were prepared per Ting et al, 2018. GABA uptake was measured by scintillation counts after incubating slices in H3-GABA for 10 minutes at 37 C. Evoked and spontaneous inhibitory postsynaptic currents (eIPSCs and sIPSCs) were recorded at 32 C and room temperature, respectively, in whole cell patch clamp configuration in presence of glutamatergic blockers 50 µM AP5 and 10 µM NBQX, after which.30 µM bicuculline was added to distinguish tonic current as a baseline shift. Results: We found reduced GABA uptake in most brain regions in 2-4 month old (mo) Slc6a1+/S295L mice compared to wildtype (WT) siblings. Surprisingly, we did not find a change in GABAergic tonic currents in pyramidal neurons of layer 6 somatosensory cortex (L6) in 2-4 mo and 7+ mo Slc6a1+/S295L and Slc6a1 S295L /S295L mice, or in ventrobasal thalamic neurons in 1 mo Slc6a1+/S295L mice compared to WT siblings. However, we did find a reduction in sIPSC frequency in L6 pyramidal neurons of 2-4 mo Slc6a1+/S295L mice. eIPSCs in L2 pyramidal neurons elicited by L4 stimulation showed a progressive increase in area under the curve and lingering current in 2-4 mo Slc6a1+/S295L and Slc6a1 S295L /S295L mice, respectively, compared to WT siblings. Conclusions: We found that brain slices from Slc6a1+/S295L mice exhibit significantly reduced GABA uptake, corroborating our in vitro and GAT-1 expression data. In agreement with this observation, we saw a prolonged GABAergic current in eIPSCs. Additionally, we observed a decrease in sIPSC frequency. Despite our hypothesis, reduced uptake did not result in increased GABAergic tonic current, but this could be due to a limitation of recording at room temperature. Together, these observations indicate a change in GABAergic neurotransmission that could be the core pathologic dysfunction in SLC6A1(S295L) patients, but currently requires further investigation.

8B. Characterization of Mycobacterium Tuberculosis – Bacillus Calmette-Guerin Using Surface Enhanced Raman Spectroscopy
Timothy W. Yokley

Tuberculosis (TB) is the second leading cause of death by an infectious disease as defined by the World Health Organization (WHO). While TB is curable, only 5-10% of people infected with TB will develop symptoms, which can lead to untimely or misdiagnosis of the disease. Moreover, people with weakened immune systems, such as the cases with HIV, latent TB is difficult to detect due to the inaccuracy of the immuno-based assays. While rapid diagnostic TB tests exist, accuracy across all types of TB infections lack sensitivity. With this in mind, the WHO has committed to ending the TB epidemic by 2030, thus; the development of culture-free, rapid diagnostic/prescreening tests are needed. Herein, this study demonstrates the ability to detect biochemical features of Mycobacterium Tuberculosis – Bacillus Calmette-Guerin (BCG), an attenuated form of TB, by ways of surface enhanced Raman spectroscopy (SERS). SERS measurements using citrate-capped gold nanoparticles (AuNPs) to evaluate biochemical features of the cell wall are shown. Preliminary results show enhancement of these cell wall features using SERS may provide a significant role for the detection of the TB bacteria from a complex matrix, such as saliva. The platform has the potential to translate into an innovative technology to screen for TB at the point-of-care.

10B. Genetically determined body fat percentage affects kidney function via the proteome
Jefferson L. Triozzi

Background: Obesity is an established risk factor for kidney disease, although underlying mechanisms are unclear. We leverage genome-wide association study data to identify molecular pathways linking body fat percentage, changes in circulating proteins, and estimated glomerular filtration rate. Methods: A two-step, multivariable Mendelian randomization and mediation analysis was performed using genome-wide association study summary statistics for body fat percentage (UK Biobank), the circulating proteome (deCODE) and estimated glomerular filtration rate (MVP and CKDGen). In the first step, genetically predicted body fat percentage is assessed for its effect on circulating proteins. In the second step, body fat-driven proteins are assessed for their effect on estimated glomerular filtration rate in both MVP and CKDGen. Heterogeneity, pleiotropy, and reverse causality are evaluated in each step. Significant findings based on deCODE proteomics were replicated using AGES-Reijeivk and FENLAND proteomics. Colocalization is used to support potentially causal pathways. Results: There were up to 665,278 participants within MVP and CKDGen Consortium with eGFR measurements included in the primary analysis. In the first step, we identified 369 proteins that were significantly affected by body fat ($p < 1.02E-05$) without heterogeneity ($I2 < 50\%$), pleiotropy (MR-Egger intercept $p > 0.05$), or reverse causation (Steiger $p > 0.05$). In the second step, we identified a significant relationship between the protein inhibin beta b and estimated glomerular filtration rate (MVP $\beta = -0.061$, SE 0.0071, $p = 7.5E-18$ and CKDGen $\beta = -0.014$, SE = 0.0027, $p = 8.3E-8$). This was replicated using cis-pQTL from the AGES-Reykjavik ($p = 9.2E-18$ and CKDGen $p = 1.8E-7$) and FENLAND ($p = 9.2E-18$ and CKDGen $p = 1.8E-7$). Colocalization show the genetic variant rs17050272 is shared between inhibin beta b

levels and estimated glomerular filtration rate (posterior probability >99%). Conclusions: The relationship between adiposity and decreased kidney function may be partially mediated by increased circulation of inhibin beta b.

12B. Fast Fuzzy C-Means Segmentation for Keypoint based Differentiation of Homogenous and Speckled Cellular Shapes
Kanchana Devanathan

Autoimmune disease is a medical condition which is caused by immune system dysfunction resulting in the healthy tissue degradation. Indirect Immunofluorescence (IIF) Imaging is the standard screening test for diagnosis of autoimmune diseases. Visual interpretation of the staining patterns is a challenging task and hence there is a growing demand for automated analysis of IIF images. Homogenous and speckled shapes are often misclassified due to their geometric similarity. Differentiation of these two patterns is essential in clinical environment since each pattern is indicative of specific autoimmune disease. In this study, an attempt has been made to differentiate the homogenous and speckled shapes using Fast Fuzzy C-Means (FFCM) segmentation and Bag-of-Keypoints (BoK) model. HEp-2 specimen images for this study are considered from the publicly available ICPR-2016 dataset. The images are preprocessed using edge-aware Local Contrast (LC) enhancement technique. After preprocessing, FFCM algorithm is implemented to segment the foreground cellular objects. Speeded up Robust Feature (SURF) Keypoint features are extracted for the pre-processed images before and after segmentation. BoK model is implemented to generate visual vocabulary from the pre-processed images with and without segmentation. A 500-word visual vocabulary is generated and is fed to k-Nearest Neighbour (kNN) classifier for classification. 10-fold cross validation is carried out to obtain optimal performance of the classifier. Results indicate that LC contrast enhancement has increased the cell structure visibility of the IIF images. FFCM segmentation has improved the detection of SURF Keypoints in IIF images. The proposed approach is able to clearly differentiate the complex and often misinterpreted shapes in IIF images. Hence this approach could be useful in computer assisted diagnosis of autoimmune diseases.

14B. Social Experiences and Mental Health Outcomes Among Autistic LGBTQ+ Youth
Natalie Libster

Introduction: Youth who identify as autistic and those who identify as LGBTQ+ are at increased risk of experiencing peer victimization, exclusion, and internalizing symptoms (Adams et al., 2014; Bottema-Beutel et al., 2019; Moran et al., 2017). These two identities often overlap, as greater gender and sexual orientation diversity is found in the autistic population than in the general population (Dewinter et al., 2017). The double minoritized identities of autistic LGBTQ+ youth may exponentiate their risk of having negative peer experiences and poor mental health (Strang et al., 2023). This study examined whether certain social experiences are associated with depression and psychological quality of life (QoL) among autistic youth, and whether the impact of these experiences on mental health differs across sexual and gender minority groups. Methods: Autistic youth (N=207) between 15-25 years old (M=18.65) with IQ above 70 participated in the current study. Data for the current analysis was collected via online survey. Participants completed a demographic questionnaire that included their biological sex, gender, and sexual orientation. Responses were coded into one of three gender/sexual identity groups: 1) Cisgender heterosexual (n=128; 108 male); 2) Cisgender non-heterosexual (n=61; 42 male); and 3) Gender-sexual minority (n=18; 7 male). Participants further completed questionnaires measuring various social experiences, including school liking and avoidance (School Liking and Avoidance Questionnaire; Ladd et al, 2000), victimization (Schwartz Peer Victimization Scale-Revised; Schwartz et al., 2002), and being ignored (Ostracism Experiences Scale for Adolescence; Gilman et al., 2013). Finally, participants completed measures of depression (Beck Depression Inventory-II; Beck et al., 1996) and psychological QoL (WHOQoL-BREF; 1998). Linear regression and moderation analyses were conducted. Sex, age, IQ, and autism symptom severity were included as covariates. Results: Depression and psychological QoL were significantly related to school liking (b=-1.09, p<.001; b=0.32, p<.001), school avoidance (b=1.06, p=.03; b=-0.37, p=.007), victimization (b=3.00, p=.005; b=-0.85, p=.006), and being ignored (b=0.32, p<.001; b=-0.10, p<.001). Compared to cisgender heterosexual participants, both cisgender non-heterosexual and gender-sexual minority participants reported lower levels of school liking (b=-2.50, p=.04; b=-5.22, p=.003) and psychological QoL (b=-1.38, p=.02; b=-3.10, p<.001). Gender-sexual minority participants also reported greater victimization (b=0.54, p=.04) and depression (b=10.70, p<.001) than cisgender heterosexual participants. Moderation analyses suggested that depression among gender-sexual minority participants was significantly more impacted by victimization compared to depression among cisgender heterosexual participants (b=5.80, p=.03). Discussion: This study highlights the importance of school-based interventions to increase school liking and positive peer experiences among autistic youth. These interventions are especially crucial for LGBTQ+ autistic youth, who are at increased risk of experiencing victimization, negative feelings about school, and poor mental health.

16B. Privacy-preserving collection and sharing of unbiased human voice data for automatic assessment of voice disorders
Zhiyu Wan

Privacy-preserving collection and sharing of voice data from patients can accelerate the automatic assessment of voice disorders. Health databases such as the Research Derivative at the Vanderbilt Medical Center cover only a certain geographical region and a certain subpopulation. To improve health equity, data-sharing initiatives such as the “All of Us” Research Program target a broader population and focus on underrepresented populations and minority groups. However, limited voice data from patients have been collected and shared in these programs. Automatic tools based on user-provided voice data are helpful for screening and monitoring symptoms and curative effects of patients with voice disorders. The data

collected from diagnosed patients are essential for learning models behind these tools. However, sharing labeled data from any single clinical site is challenging due to legal and privacy issues. Voice data are potentially identifiable especially when companies like Apple and Amazon have collected massive amounts of voice data through their virtual assistants. The fact that demographics, genomic data, and medical histories are usually shared along with patients' voice data brings more risks. An attacker can use external data to re-identify the shared data. We aim to propose anonymization methods for expanding voice data sharing without compromising patients' privacy. To do so, we first evaluate the privacy risks of sharing patients' voice data and then examine existing anonymization methods for voice data sharing in a healthcare scenario. Nonetheless, changes made to the original data may harm downstream usages of the data. We use modern automatic speaker verification models to assess privacy risks. The data utility is evaluated as the F1 score of a state-of-the-art deep learning model for dysphonia detection. To anonymize voice data, we first extract features including X-vector features and non-X-vector features, and then we synthesize voice by replacing the X-vector features. Using data from 2,500 people, experimental results show that our anonymization method can expand access to patients' voice data while preserving privacy and the effectiveness of downstream clinical usage.

18B. Adolescent-onset voluntary ethanol consumption and subsequent negative affective behavior and whole brain cFos expression during forced abstinence in mice

Caitlyn Edwards

Negative affect experienced during abstinence from alcohol can significantly contribute to relapse and the development of alcohol dependence. In particular, chronic alcohol use during adolescence poses a substantial risk for the later development of alcohol use disorder. This study aimed to investigate the voluntary consumption of ethanol and its impact on negative affective behavior, as well as associated neural changes, in mice that initiated ethanol consumption during early adolescence (~PND30). Male and female adolescent C57BL/6J mice went through the Chronic Drinking Forced Abstinence (CDFA) paradigm in which half of the mice ("Ethanol" group) were given two-bottle choice between ethanol and water whereas the control mice ("Water" group) were given two bottles containing water. In Experiment 1, ethanol bottle weights were manually recorded to measure ethanol intake (g/kg/day) and ethanol preference over a six-week period. Subsequently, the bottles were removed, and two weeks later, the animals underwent several behavioral tests to evaluate negative affect. While female mice prefer and consume more ethanol than males as adults, we found that male and female mice that began drinking during early adolescence consume similar levels of ethanol and display similar preference for ethanol over water. We also observe negative affective behaviors in mice during forced abstinence. In Experiment 2, ethanol intake was assessed using the Lick Instance Quantifier (LIQ) system, enabling a more precise measurement of ethanol consumption behavior, including lick number and lick duration. Additionally, brains were collected at 24 hours and 2 weeks into forced abstinence and analyzed for regionally specific changes in whole brain cFos expression. Adolescent onset of CDFA provides a translationally relevant model of negative affect following chronic alcohol consumption and could provide interesting insight into neural circuitry underlying the development of alcohol use disorder.

20B. Correlates of Self-Reported Life Satisfaction in Autistic Youth with and without Intellectual Disability

Carly Moser

Background: The identification of meaningful outcomes for autistic people is necessary to optimize supports that align with the population's needs. While outcomes for those with autism have historically focused on objective indicators of well-being (e.g., social participation, employment), a greater emphasis on subjective measures of well-being, including life satisfaction, is a high priority for the autistic community1. Research examining factors that promote life satisfaction is limited, and existing studies do not include the perspective of autistic people with intellectual disability (ID). Therefore, the present study aims to expand current research by identifying correlates of self-reported life satisfaction in autistic youth with and without ID. Specifically, the study examined associations between life satisfaction and youth characteristics (mental health, self-determination), parent characteristics (mental health), and objective indicators of well-being (social participation, unmet service needs). Methods: Participants were 134 autistic youth (M = 19 years) enrolled in a larger randomized controlled trial. Data for this study was collected at baseline. Life satisfaction was measured using the Satisfaction with Life Scale2, a five-item self-report survey. Youth mental health was measured using the DSM-oriented anxiety and depression scales of the Child Behavior Checklist3/Adult Behavior Checklist4, a parent-report survey. Youth self-determination was measured via the Self Determination Inventory System5, a self-report survey. Parent mental health was measured using the Depression Anxiety Scales questionnaire6. Social participation and unmet service needs were measured using questions from the National Longitudinal Transition Study-2. The frequency of the youth's current social activities and the number of unmet service needs were used in the analysis. Results: Separate correlation matrices were computed for autistic youth with ID (n=37) and youth without ID (n=97) to identify unique correlates of life satisfaction across the groups. Life satisfaction was significantly associated with youth depression ($r = -.36$, $p<.001$) and self-determination ($r=.61$, $p<.001$) for autistic youth without ID. Life satisfaction was significantly associated with parental anxiety ($r=-.50$, $p= .002$), parental depression ($r=-.45$, $p= .006$), social participation ($r=43$, $p= .008$), and unmet service needs ($r=-.60$, $p< .001$) for autistic youth with ID. No other factors were associated with life satisfaction for either group (ps>.09). Discussion: In the current study, life satisfaction in autistic youth without ID was associated with personal characteristics, whereas life satisfaction was associated with parent characteristics and objective indicators of well-being for autistic youth with ID. Our findings demonstrate unique differences in factors related to positive outcomes for youth with and without ID and emphasize the need to consider the heterogeneity across individuals on the autism spectrum when assessing how to best support positive outcomes in this population.

Abstracts
Poster Presentations

22B. Static storage at 10°C improves biliary viability in porcine donation after cardiac death livers
Kaitlyn M. Tracy

Background: Access to machine perfusion technology remains limited given logistical and financial hurdles. Optimized conventional static cold storage could be broadly implemented and potentially improve organ quality. Methods: A porcine donation after cardiac death (DCD) model was developed to mimic human DCD. After standard procurement, the liver was placed in static storage for 12 hours at 10°C, 18°C, or on ice, with n=1 per group. Allograft function was subsequently evaluated on a normothermic machine perfusion (NMP) platform with autologous porcine blood over 4 hours. Results: Lactate normalized within 2 hours of NMP for livers stored on ice and at 10°C. Throughout NMP, the liver stored at 10°C produced 24.5mL of bile compared to 8.0mL and 15.4mL for livers stored on ice or 18°C, respectively. The highest biliary pH (7.31) and HCO3- (10.8 mmol/L) were demonstrated after 10°C storage compared to livers stored on ice or 18°C. For the liver stored at 10°C, histologic evaluation of the common bile duct after NMP demonstrated superior preservation of structures predictive of ischemic cholangiopathy, quantified as a histologic injury score of 3 out of 7 compared to scores of 7 and 5 for ice and 18°C, respectively. Conclusion: Livers stored on ice and at 10°C demonstrated similar hepatocellular function, however, established biliary biomarkers and histologic injury markers were most favorable after storage at 10°C. These data suggest improved biliary viability after 10°C storage compared to conventional storage on ice, which is of particular importance in DCD allografts.

24B. Rapid handheld measurements of skin and subcutaneous tissue stiffness in Systemic Sclerosis: a case series
Shramana Ghosh

Noninvasive quantitative assessment of skin for assessing the severity of cutaneous Systemic Sclerosis (SSc) remains a clinical need. The Myoton device has considerable potential for rapidly and accurately assessing cutaneous sclerosis through measurement of skin biomechanical properties. We used the Myoton to measure skin stiffness of three SSc patients, each with different disease types: limited (48 y, F), diffuse-active (21 y, M), and diffuse-late (52 y, M). Eight sites were measured on the upper limbs of each patient (bilateral shoulders, biceps, dorsal and volar forearms). At each measurement site, skin and subcutaneous thickness were also calculated from B-mode images obtained with a VevoMD High-frequency Ultrasound device with a 48MHz probe. Median values were compared with a Wilcoxon rank sum test. Median Myoton stiffness across all 8 sites of the patient with active disease was 686 N/m [IQR: 564 – 981 N/m], which was significantly higher than that of the patients with limited SSc (350; IQR 327-410 N/m, $p<0.01$) and late disease (472; IQR 422-587 N/m, $p<0.05$). Similarly, the median skin thickness of the patient with active disease (2.22; IQR: 1.90 – 2.42 mm) was significantly higher than the patients with limited or late disease ($p<0.05$). Median subcutaneous thickness in the patient with active disease (3.66; IQR: 2.97 – 4.30 mm) was lower compared to the patients with limited ($p<0.01$) or late ($p=0.21$) disease. Across all 24 measured sites of the three subjects, Myoton stiffness had high correlation with subcutaneous tissue thickness (Spearman $\rho = -0.92$, $p <0.001$). This was far higher than the correlation of stiffness with skin thickness ($\rho = 0.30$, $p=0.15$), or of prior reports of correlation of Rodnan scores with skin thickness ($\rho = 0.00$ to 0.72 in literature). Myoton stiffness measurements may be a useful method to distinguish between and follow limited, active, and late disease and show unprecedented correlation to subcutaneous anatomy in SSc.

26B. Proteomic Alteration in T1DM: Insights into Cardiometabolic Complications and Hyperinsulinemia-Driven Insulin Resistance.
Naweed Akbar

From every aspect, I profoundly think this project is highly worth studying and working on. We know that T1DM has more deleterious effects on the cardiovascular system than T2DM hence I like to do my research on how T1DM affects endothelial cells and what the other factors that contribute to the initiation of complications. This research will help me to understand the details of the glucose clamp technique, which is unique and more useful tool for analyzing glucose concentration and lactate. I had my first glucose clamp technique at the end, I learned many things and other related issues. In addition, the glucose clamp technique, we are fulfilling FMD (Flow-mediated dilation). With FMD, we assess how endothelial cells dilate before and after giving the patients nitroglycerin. This is a non-invasive technique and very useful for evaluating the endothelial cell function. As my project progress further and meets the expectations of my mentors and PI, I will work on proteomic protein studies approach and how they explore alterations induced by insulin and initiation of cardiovascular complications such as atherosclerosis. We are conducting and studying proteomic protein in normal subjects, GCK-MODY and T1DM. Cardiovascular disease (CVD) is a significant complication in the management of Type 1 diabetes mellitus. Even when glycemic control is achieved, individuals with T1DM face a higher CVD than healthy individuals and those with maturity-onset diabetes of the young (GCK-MODY), a monogenic form of diabetes. Intriguingly, GCK-MODY patients do not share the same elevated CVD risk, despite lifelong hyperglycemia, indicating that factors beyond glucose levels are involved. The study aims to explore proteomic alterations induced by insulin and to understand the different CVD risk profiles among these groups, especially focusing on the potential role of iatrogenic hyperinsulinemia as a major contributor to insulin resistance in T1DM.

28B. Neurobiological Underpinnings of Discourse Understanding: Integra7ve Insights from fMRI and EEG
Clair Hong

Approximately 43 million U.S. adults struggle with basic text comprehension. Despite a wealth of research exploring the neural underpinnings of reading disorders in children, reading comprehension in adults remains under-studied. This study fills the gap, applying highresolution fused MRIEEG

analysis to identify neural mechanisms underlying reading comprehension in adults with varying range of reading abilities. We examined typical adults as they read medical passages in the MRI, and in a separate session, while EEG data was collected. Joint Independent Component Analysis (ICA) revealed comprehension variations associated with differences in network exchanges related to word reading and oral language between groups with lower and higher reading comprehension abilities, with early and late signals involved. These exchanges interacted with executive function regions, aligning with the Simple View of Reading model. This study underscores the complexity of neural network interactions in adult reading comprehension and suggests potential avenues for developing targeted interventions catered to adults with varying levels of reading comprehension ability. This investigation offers crucial contributions to our understanding in the field of neuroscience and brain-based reading comprehension interventions.

30B. Effect of Pediatric Doses of Atomoxetine on Presyncope Symptoms in Neurogenic Orthostatic Hypotension: A Randomized, Double-blind, Placebo-Controlled, Crossover, Clinical Trial

Naome Mwesigwa

Context: neurogenic orthostatic hypotension (NOH) is associated with syncope, falls and poor quality of life. Treatment is challenging because of few therapeutic agents. Atomoxetine, a norepinephrine transporter inhibitor, improved upright blood pressure and symptoms in NOH. However, the long-term efficacy of atomoxetine for the treatment of NOH is unknown. Objective: To determine the efficacy of chronic treatment with 18 mg atomoxetine on pre-syncopal symptoms in NOH patients Design, Setting, and Subjects: Randomized, double-blind, placebo-controlled, two period crossover trial, conducted between July 2016 and May 2021 in two national autonomic referral centers in 40 NOH patients. Interventions: 4-week treatment sequence (period 1: atomoxetine (10 or 18 mg BID) followed by placebo) or vice versa (period 2), separated by a 2-week washout period. Main Outcome Measures: orthostatic hypotension questionnaire (OHQ) composite score assessed at day 0,14,28,36,50 and 64. OHQ composite score was average of OHSA (orthostatic hypotension symptom assessment) and OHDAS(orthostatic hypotension daily activity scale) Results: 40 NOH patients were recruited, 60% men, 37 completed the trial, mean age 67.9 ±8.1, 41% met criteria for Multiple System Atrophy. OHQ composite score was similar between placebo and atomoxetine treatment (-0.31±1.66 vs -0.39±1.48, p=0.806) at 2 weeks and (-0.58±2.39 vs -0.5±1.58, p=0.251 at 4 weeks). Ohsa of atomoxetine vs placebo was (2.77±2.2 vs 2.9±2.15) at 4 weeks and ohdas was (4.15±2.95 vs 3.8±2.71). Atomoxetine was well-tolerated, and no significant adverse events were reported with atomoxetine. Conclusions: Atomoxetine did not have any effect on OH-symptoms and falls.

32B. Imaging of Metabolites in Human Ocular Tissue by Mass Spectrometry

Ali Zahraei

Introduction: Glucose, as a primary nutrient, is essential to drive the functional processes that actively maintain lens transparency and meet the high metabolic demand of the retina. Once glucose is taken up by a cell, it can be utilized in multiple metabolic pathways, including glycolysis, the pentose phosphate pathway, the polyol pathways, and glycogen synthesis. However, there is a lack of understanding of the localized metabolism occurring in the eye under normal conditions. Therefore, this study aims to optimize sample preparation methods for matrix-assisted laser desorption/ionization imaging mass spectrometry (MALDI IMS) to precisely visualize the distribution of metabolic pathways in normal human eyes. MALDI IMS is a powerful tool for systems biology studies, offering high sensitivity and label-free capabilities, providing comprehensive spatial distribution of multiple classes of biomolecules. The application of MALDI IMS to the study of endogenous compounds has received considerable attention because permutations in metabolic pathways can be indicative of pathology and disease. Thus, MALDI IMS can enhance the understanding of disease mechanisms and elucidate mechanisms for biological variation. Methods: A whole human ocular globe was frozen using liquid nitrogen vapor in 15% fish gelatin. The globe was then dissected into anterior and posterior portions. Both regions were cut and thaw-mounted onto indium tin oxide-coated glass slides covered with Poly-Lysine. Autofluorescence microscopy images were acquired before IMS analysis. N-(1-Naphthyl) ethylenediamine dihydrochloride was used as a matrix and applied using an HTX M5 Sprayer device. Data were acquired with a 10 µm pixel size in negative ion mode, covering a mass range of 100-1000 Da. The metabolomics MALDI-IMS data were acquired using a Bruker timsTOF Flex in QTOF mode. Preliminary Data: A wide variety of tissue metabolites were imaged at high spatial resolution. These include sugars, intermediates in redox and methionine metabolism, nucleotides, and intermediates within the central carbon metabolism pathway. The high spatial resolution data allowed determination of the spatial distributions of different endogenous compounds in the lens, ciliary body, iris, and cornea. Furthermore, it enables differentiation of the multiple cell types present in retinal layers and the optic nerve. These findings significantly contribute to our understanding of metabolic dynamics within the eye. Highlights: Multimodal imaging of human eye tissues provides a comprehensive view of how metabolites impact normal vision. This work also establishes a consolidated research pipeline for studying 3-D biomolecular multimodal tissue imaging, enabling the creation of high-resolution metabolite images of the human eye in future research endeavors.

34B. Glutaminase Promotes Amino Acid-Induced Alpha Cell Proliferation.

Madushika Wimalarathne

Interrupting glucagon signaling in the liver reduces blood glucose levels in animal models and individuals with diabetes. However, interrupting glucagon signaling also leads to hyperaminoacidemia and proliferation of glucagon secreting a-cells, evidence of an endocrine liver-a-cell axis. High

glutamine levels are required for a-cell proliferation. We recently found that glutaminase (Gls/GLS) is expressed in a-cells at much higher levels than any other pancreatic endocrine cells including a high-capacity mitochondrial isoform GAC. To test the role of glutamine metabolism in a-cell proliferation, GLS activity was specifically knocked out in mouse a-cells (a*Gls*^{KO}). Targeted deletion of *Gls* expression in most a-cells was confirmed by staining for GLS and glucagon (a*Gls*^{WT}: 95% GLS^{+}; a*Gls*^{KO}: 18% GLS^{+}). Mice were treated with a glucagon receptor monoclonal antibody (GCGR mAb) for 10 days or with isotype control IgG. Pancreases were collected and stained for glucagon to identify a-cells along with a proliferation marker Ki67. As previously shown, a*Gls*^{WT} mice treated with GCGR mAb have robust a-cell proliferation while a*Gls*^{KO} mice treated with GCGR mAb for 10 days showed a 4.5-fold decrease in a-cell proliferation and were similar to mice treated with the control IgG (a*Gls*^{WT} Ab: 17.0 ± 4.6% a-cell proliferation, a*Gls*^{WT} IgG: 1.0 ± 0.4%*A***, a*Gls*^{KO} IgG: 0.2 ± 0.2, a*Gls*^{KO} Ab: 3.8 ± 1.6%**; n=4-6, **p < 0.01). In addition, a*Gls*^{WT} mice treated with GCGR mAb show a robust activation of mTOR in a-cells while this is lost in a*Gls*^{KO} mice treated with GCGR mAb. Together these data suggest a critical role for glutamine metabolism via glutaminase in a-cell proliferation.

36B. Dynamic organ storage at 10°C improves cholangiocyte function compared to static cold storage
Yutaka Shishido

Donation after cardiac death (DCD) livers are vulnerable to ischemic cholangiopathy. During organ storage, oxygen delivery is thought to mitigate ischemic injury. Moreover, static storage at 10°C has been suggested to preserve mitochondrial health better than conventional cold storage (CS) on ice. Herein, we hypothesize that continuous delivery of oxygen at 10°C will improve liver graft function compared to CS. Given the logistical complexity of machine perfusion, we aimed to deliver oxygenated perfusate with only pressure bags and manual flow regulators (Figure 1). In a porcine DCD model, procured livers were stored by CS or dynamic storage (DS) at 10°C for 12 hours and graft function was evaluated using Normothermic Machine Perfusion (NMP), with n=1 per group. Oxygenated UW machine perfusion solution with autologous porcine blood was used to perfuse the liver for DS. Perfusate flows were 95 mL/hr and 154 mL/hr to the hepatic artery and portal vein, respectively. Liver effluent from the hepatic veins showed a decrease in AST, ALT, and LDH from 2031 U/L, 350 U/L, and 2450 U/L to 180 U/L, 27 U/L, and 432 U/L, respectively, after 12 hours of DS (Figure 2). DS liver showed superior biliary biomarkers (bile pH: 7.32, bile/perfusate glucose ratio: 0.20) compared to CS liver (bile pH: 7.16, bile/perfusate glucose ratio: 0.50) after 4 hours of NMP. Our simple DS circuit at 10°C could better protect cholangiocyte function during storage and be used to assess organ viability.

38B. The EaRTH Disk Model: Analyzing Millimeter and Infrared Observations of Disk Substructures of Transitional Disks
William Grimble

To understand how exoplanets form and evolve, we must understand the protoplanetary disks where they are born. Such an understanding relies on analyses of both the mineralogy of protoplanetary disks and their detailed structures; however, these key complementary aspects of disks are often studied separately. In a previous paper, we developed and demonstrated a hybrid analysis of these aspects we called the EaRTH Disk Model. While the model can successfully match known observation assuming a typical fiducial protoplanetary disk such as MP Mus, it is necessary to alter the model to match data when structural differences are observed, such as a gap or rings; adjusting the model to match infrared observations while remaining consistent with millimeter observations demonstrates the model's adaptability to different disk structures, which we do using the Spitzer IRS spectra and Atacama Large Millimeter/sub-Millimeter Array (ALMA) observations of a set of 20 transitional disks, including GM Aur and LkCa 15. The results illustrate the large differences that occur in protoplanetary disk development despite similar ages, likely the result of planetary formation.

40B. Cognitive empathy anosognosia relates to social vulnerability in behavioral-variant frontotemporal dementia
Jayden J. Lee

Background: Risk for financial exploitation, also known as social vulnerability, is a devastating but common problem among the elderly, reported to lose an estimated $3 to $36 billion annually to financial scams. Older adults with dementia are particularly susceptible to falling victim to financial fraud. However, it remains unknown whether cognitive or socioemotional impairment is associated with increased social vulnerability in neurodegenerative diseases. The present study examines the relationship between impaired empathy and self-awareness (i.e., anosognosia) in Alzheimer's disease (AD) and behavioral-variant frontotemporal dementia (bvFTD). Methods: 20 AD and 10 bvFTD patients were included in this study. Social vulnerability in patients was assessed by administering to their caregivers the Social Vulnerability Scale (SVS), a 15-item informant-based questionnaire, comprising two factors of social vulnerability (gullibility and credulity). Empathy was measured using the Interpersonal Reactivity Index (IRI) questionnaire, specifically the two subscales for perspective-taking (cognitive empathy) and empathic concern (emotional empathy). We evaluated patients' unawareness of their own empathy by administering the IRI to both patients and caregivers and computed difference scores for perspective-taking and empathic concern (patients' score minus the caregivers' score). Group-level differences were measured using one-way ANCOVA tests, controlling for age, sex and disease severity, and general linear regression models were performed to determine associations between empathy assessments and social vulnerability. Results: Informant ratings for gullibility, credulity, and total social vulnerability were significantly higher in bvFTD compared to AD patients. Cognitive and emotional empathy ratings were significantly lower in bvFTD than AD. Patients' assessments of their own perspective-taking capability were associated with increased gullibility and credulity in both groups. Critically, the discrepancies between patients' own assessments and their caregivers' in both perspective-taking and empathic concern were significantly greater in bvFTD compared to

AD, i.e., bvFTD patients showed greater deficits in self-awareness of empathy capability than AD patients. Within bvFTD, the discrepancy in perspective-taking capability assessment was significantly associated with increased credulity, a factor of social vulnerability. Conclusions: Our results suggest that social vulnerability is a greater problem in bvFTD than AD and distinctly related to patients' unawareness of their own perspective-taking capability. Perspective-taking, or the ability to understand or adopt another person's perspective, is a central component of cognitive empathy. bvFTD patients' cognitive empathy anosognosia may potentially be considered as an early risk factor for social vulnerability.

42B. Elucidating the Role of Activated Leukocyte Cell Adhesion Molecule (ALCAM) in the Biogenesis and Function of Tumor Extracellular Vesicles
Javier Ramirez-Ricardo

ALCAM is a transmembrane glycoprotein that belongs to the immunoglobulin superfamily of cell adhesion proteins. It is expressed in various cell types, including cancer cells, regulating the dynamic turnover of adhesions to contribute to cell motility and metastasis. Given the critical emerging roles of extracellular vesicles (EVs) in regulating cancer cell migration and metastasis, we asked whether ALCAM might impact EV biogenesis, composition, or function to control migration, invasion, and metastasis, which are critical in cancer. To study the effects of ALCAM on cancer cells, we generated ALCAM-deficient SW780 and UMUC3 bladder tumor cell lines using CRISPR-Cas9. EVs were isolated from control and ALCAM knockout cell culture supernatants by serial ultracentrifugation to generate 10,000g and 100,000g pellets. Nanoparticle tracking (ZetaView), western blots, and a bead-based flow cytometry array were performed. Although no differences were observed in EV counts between SW780 WT and ALCAM deficient cells, we detected by western blot reduced amounts of Alix, Flot-1, and high expression of Syntenin and TSG101 in the lysates of 100,000g pellets of SW780 ALCAM-deficient cells. In contrast, CD9 and CD151 expression was preserved. Moreover, the bead-based flow cytometry array identified differences in the epithelial and immune markers in EV populations between control and ALCAM-deficient cell lines. These data suggest that the protein composition of EVs secreted by control cells differs from that of ALCAM-KO cells. Future studies will investigate how the loss of ALCAM may alter EV biogenesis and cargo loading and test whether this has a functional impact on bladder cancer progression.

44B. Intralaboratory Evaluation of a Quality Control Workflow across Identical LC-MS/MS Systems
Khiry L. Patterson

Large-scale plasma proteomics analyses include multiple steps such as sample preparation, fractionation, and liquid chromatography tandem mass spectrometry (LC-MS/MS). Experimental variability can occur at any step thus requiring the need for a quality control (QC) workflow to ensure optimal instrument performance and to avoid costly delays. Additionally, it is necessary to generate comparable data for proteomics analyses especially when similar instrumental systems are used. Previously, we established a LC-MS/MS QC workflow that utilizes a series of analytical metrics such as m/z tolerance (%m/z), peptide and protein counts, peptide spectral matches, and number of MS/MS spectra to monitor daily instrument performance. The goal of this study was to evaluate the performance of the QC workflow on two identical LC-MS/MS systems based on an Orbitrap Q-Exactive (QE) MS instrument. Similar QC samples of human plasma were subject to replicate injections (N = 30) on both systems and monitored daily for instrument performance. Across the two systems, we observed comparable numbers of protein identifications (i.e. 328 proteins), peptide identifications (i.e. 3030), peptide spectral matches (8288), MS/MS spectra (i.e. 55903), and %m/z (i.e. 99.80%). Tracking peptide retention times were observed to be left-shifted by ~ 3 minutes from QE1 to QE2. Furthermore, the analysis suggests that the chromatographic conditions require stability for both systems to yield the same results. Overall, the QC workflow implementation is helpful to ensure robust and similar performance for large-scale plasma proteomics across multiple LC-MS/MS systems within the same laboratory.

46B. Understanding the role of TET2-deficient monocytes in clonal hematopoiesis of indeterminate potential (CHIP)
Kristen Dickerson

Clonal hematopoiesis of indeterminate potential (CHIP) is an age-related somatic mosaicism that is defined by the presence of malignancy-related mutations in the hematopoietic system of individuals that lack malignancy. Loss of function mutations in the DNA methyltransferase, TET2, are one of the most common perturbations in CHIP and lead to a clonal expansion of TET2-deficient hematopoietic stem cells (HSCs) and progeny. TET2-deficient HSCs have increased self-renewal and engraftment potential, which is further intensified in the presence of inflammatory signaling. Additionally, TET2-deficient monocytes are hyperinflammatory compared to wild type monocytes. We hypothesized that TET2-deficient monocytes release inflammatory cytokines that directly suppress wild type HSC function and support TET2-deficient HSC function, which contributes to the TET2-deficient clonal expansion observed in CHIP and myeloid malignancies. To assess how TET2-deficient monocytes impact HSC function, we developed a co-culture system that utilizes transwells to culture primary mouse HSCs with primary mouse monocytes. After 48-72 hours in culture, HSC populations were analyzed for changes in immunophenotype and self-renewal capacity using CyTOF and colony forming unit assay (CFU), respectively. After 48 hours in co-culture with TET2-deficient monocytes, TET2-deficient HSCs had increased expression of stem cell markers compared to HSCs co-cultured with wild type monocytes. However, when the culture was extended to 72 hours, co-culture with TET2-deficient monocytes led to increased myeloid differentiation of the TET2-deficient HSCs. TET2-deficient HSCs have sustained self-renewal compared to wild type HSCs, however, after co-culture with TET2-deficient monocytes for 72 hours, the self-renewal ability is reduced due to myeloid differentiation. In summary, these experiments reveal that TET2-deficient monocytes alter the immunophenotype and self-renewal ability of HSCs ex vivo which could promote clonal expansion in individuals with CHIP.

THANK YOU

The 2023 VPA Symposium Committee would like to thank our partners, invited speakers, panelists, judges, and postdoc presenters for your continued support and participation.

Vice Provost Dr. Andre Christie-Mizell Keynote

Speaker Dr. Keivan Stassun

Postdoc of the Year Dr. Siru Liu

Alumni Panel Members

Dr. Whitney Taylor from the Career Center

Dr. Jessica Abner from the Career Center

Workshop Speaker Dr. Ashley Brady Faculty

Judges

Postdoc Presenters

Office of Postdoctoral Affairs

Office of Biomedical Research Education and Training

Vanderbilt Catering & Events

Vanderbilt Facilities

Organizing Committee

Annie Evans
Office of Postdoctoral Affairs

Faith Bishop
Office of Postdoctoral Affairs

Dr. Madeline Searcy
Department of Medicine
Division of Clinical Pharmacology, VUMC

Dr. Tor Nasci
Department of Medicine
Division of Nephrology, VUMC

Dr. Anwar Said
Department of Computer Science, VU

Dr. Madushika Wimalarathne
Department of Medicine
Division of Diabetes & Endocrinology, VUMC

Dr. Isabella Starling Alves
Department of Psychology and Human Development, VU

Dr. Mahima Sharma
Department of Biomedical Engineering, VU

Dr. Katherine Young
Department of Biomedical Engineering, VU

Dr. Caitlyn Edwards
Department of Molecular Physiology & Biophysics, VU

Dr. Chitra Shaji
Department of Biomedical Engineering, VU

Dr. Nadia Markie Sneed
Division of Pediatrics
School of Nursing, VU

Dr. Néstor de la Visitación
Department of Medicine
Division of Clinical Pharmacology, VUMC

Dr. Timothy Ryan Harris
Department of Cardiac Surgery, VUMC

Dr. Vanessa Cerda
Department of Psychology and Human Development, VU

Dr. Janani Varadarajan
BRET Office